

# Substantial root-zone water storage capacity observed by GRACE and GRACE/FO

Meng Zhao<sup>1</sup>, Erica L. McCormick<sup>2</sup>, Geruo A<sup>3</sup>, Alexandra G. Konings<sup>2</sup>, Bailing Li<sup>4,5</sup>

<sup>1</sup>Department of Earth and Spatial Sciences, University of Idaho, Moscow, ID 83843, U.S.

<sup>2</sup>Department of Earth System Science, Stanford University, ~~Palo Alto~~Stanford, CA 94305, U.S.

<sup>3</sup>Department of Earth System Science, University of California, Irvine, CA 92617, U.S.

<sup>4</sup>NASA Goddard Space Flight Center, Greenbelt, MD 20771, U.S.

<sup>5</sup>Earth System Science Interdisciplinary Center, University of Maryland, College Park, MD 20742, U.S.

Correspondence to: Meng Zhao (mengz@uidaho.edu)

**Abstract.** Root-zone water storage capacity ( $S_r$ ) - the maximum water volume ~~that can be held in the plant root zone~~available for vegetation uptake - bolsters ecosystem resilience to droughts and heat waves, influences land-atmosphere exchange, and controls runoff and groundwater recharge. ~~In land models,  $S_r$  serves as a critical parameter to simulate water availability for vegetation and its impact on processes like transpiration and soil moisture dynamics.~~ However,  $S_r$  is difficult to measure, especially at large spatial scales, hindering ~~an~~ accurate ~~simulations~~understanding of many biophysical processes, such as photosynthesis, evapotranspiration, tree mortality, and wildfire risk. Here, we present a global estimate of  $S_r$  using ~~direct~~ measurements of total water storage (TWS) anomalies from the Gravity Recovery and Climate Experiment (GRACE) and GRACE Follow-On satellite missions. We find that the median  $S_r$  value for global vegetated regions is at least  $220 \pm 40$  mm, which is over 50% larger than the latest estimate derived from tracking storage change via water fluxes, and 380% larger than that calculated using ~~the a typical~~ soil and rooting depth parameterization. ~~Parameterizing~~These findings reveal that plant-available water stores exceed the storage capacity of 2-meter-deep soil in nearly half of Earth's vegetated surface, representing a notably larger extent than previous estimates. Applying our  $S_r$  estimates in a global hydrological model ~~with our  $S_r$  estimate~~ improves ~~TWS and~~evapotranspiration simulations ~~compared to other  $S_r$  estimates~~ across much of the globe. ~~Furthermore, our  $S_r$  estimate, based solely on hydrological data, correlates realistically with an independent vegetation productivity dataset, underseering, particularly during droughts, highlighting~~ the robustness of our approach. Our study highlights the importance of continued refinement and validation of  $S_r$  estimates and provides a new ~~pathway~~observational approach for further exploring the impacts of  $S_r$  on water resource management and ecosystem sustainability.

## 1 Introduction

During periods of insufficient precipitation, vegetation relies on water stored underground to survive (Miguez-Macho and Fan, 2021). The larger the root-zone water storage capacity ( $S_r$ ), the more water ~~plants~~the root zone can store during wet periods for use in droughts (Teuling et al., 2006).  $S_r$ , therefore, plays an important role in regulating ecosystem resilience to

32 droughts and heat waves and affecting wildfire outbreaks and mortality risk (Callahan et al., 2022; Chen et al., 2013; Goulden  
33 and Bales, 2019; Hahm et al., 2019; Humphrey et al., 2018; Stocker et al., 2023). It is also an essential parameter for  
34 ~~modeling~~modelling plant carbon uptake, transpiration, soil evaporation, streamflow, and groundwater (Maxwell and Condon,  
35 2016; Zhao et al., 2022; Peterson et al., 2021). Despite its critical role in modulating the carbon and water cycles, global  
36 patterns of  $S_r$  remain poorly characterized.

37 The  $S_r$  is typically calculated as the integration of plant rooting depth and soil texture-dependent water-holding  
38 capacity (Seneviratne et al., 2010; Vereecken et al., 2022; Speich et al., 2018; Federer et al., 2003). However, this approach  
39 (hereafter referred to as the rooting depth-based estimation) suffers from uncertainties associated with plant rooting depth and  
40 substrate hydraulic properties, particularly at depth, ~~undermining both of which undermine~~ the accuracy of the calculated  $S_r$   
41 (Vereecken et al., 2022; Novick et al., 2022). ~~Additionally, it overlooks a significant contribution to  $S_r$  from plant roots~~  
42 ~~extracting moisture stored in weathered bedrock in the form of rock moisture.~~ Moreover, this approach assumes a static root  
43 ~~zone confined to the near surface unsaturated soil layer.~~ However, recent studies have shown that this assumption is not always  
44 ~~accurate. In many ecosystems, plant roots can penetrate beyond the shallow soil layer into weathered bedrock, accessing rock~~  
45 ~~moisture and tapping into groundwater, especially during prolonged dry periods (Li et al., 2015; Hahm et al., 2020; McCormick~~  
46 ~~et al., 2021; Rempe and Dietrich, 2018; Meeormiek Maxwell and Condon, 2016; Fan et al., 2017; Baldocchi et al., 2021) and~~  
47 ~~groundwater (Maxwell and Condon, 2016; Fan et al., 2017).~~ Thus, the rooting depth-based estimation may significantly  
48 underestimate  $S_r$ .

49 More recently, Earth observations of precipitation (P) and evapotranspiration (ET) have been used to estimate  $S_r$ .  
50 Several studies (Stocker et al., 2023; Wang-Erlandsson et al., 2016; Gao et al., 2014; ~~Meeormiek~~McCormick et al., 2021) have  
51 proxied  $S_r$  using the maximum cumulative difference in ET and P during dry periods (when ET > P), which reflects the largest  
52 water volume that an ecosystem has withdrawn from its root zone. This method (hereafter referred to as the water deficit-based  
53 estimation) is based on mass balance and thus eliminates the need for ~~information~~assumptions about plant access to rock  
54 moisture and groundwater, rooting depth, and soil and bedrock hydraulics. However, obtaining accurate P and ET data is  
55 challenging at scale (Sun et al., 2018; Miralles et al., 2016), and errors in these data can accumulate and deteriorate  $S_r$   
56 calculations. Here, to avoid this shortcoming, we estimated root-zone storage dynamics directly from total water storage (TWS)  
57 anomalies measured by the Gravity Recovery and Climate Experiment (GRACE) and GRACE Follow-On (GRACE-FO)  
58 satellite missions (hereafter GRACE/FO). With these ~~direct~~ observations, we characterized global patterns of  $S_r$  and found that  
59 both the rooting depth-based estimate and the water deficit-based estimate have significantly underestimated  $S_r$ .

## 60 2 Materials and methods

### 61 2.1 GRACE/FO TWS

62 We use monthly measurements of the TWS anomaly from GRACE for the years 2002-2017 and from GRACE-FO  
63 for the years 2018-2022. These measurements were obtained from the Jet Propulsion Laboratory (JPL) RL06 solutions

(Watkins et al., 2015; Wiese et al., 2016), which provide monthly average anomalies of the gravity field over an equal-area  $3^\circ \times 3^\circ$  mass concentration block (mascon). We opted for the JPL mascon solutions because each JPL mascon is relatively uncorrelated with ~~neighboring~~neighbouring mascons and thus offers more localized spatial variations than other mascon solutions and the spherical harmonic solutions (Watkins et al., 2015; Wiese et al., 2016). We did not fill the 11-month gap (July 2017 to May 2018) between GRACE and GRACE-FO. However, we linearly interpolated other missing months from the nearest previous and subsequent non-missing values (Rodell et al., 2018; Zhao et al., 2021). Because we aimed to estimate root-zone storage capacity  $S_r$ , we only included mascon locations with over 50% fractional vegetation cover based on the land cover product (MCD12Q1) version 6.1 from the Moderate Resolution Imaging Spectroradiometer (MODIS) (Sulla-Menashe and Friedl, 2018).

## 2.2 $S_r$ from TWS drawdown and uncertainty estimate

Ecosystem use of land water storage for ET is ~~represented~~reflected in ~~the~~-TWS ~~drawdown, that is, a~~drawdowns, consecutive ~~declined~~declines in TWS ~~anomaly~~-despite seasonal or intermittent recharge and after accounting for long term trend due to anthropogenic groundwater use. An example is illustrated in Fig. 1 at a mascon location in southern Idaho, where the largest TWS drawdowns are annotated. From the water balance, a TWS drawdown over a time-period  $\Delta t$  is equal to:

$$\Delta TWS = \sum P - \sum ET - \sum R \quad (1)$$

where  $\sum P$ ,  $\sum ET$ , and  $\sum R$  are the total precipitation, total evapotranspiration, and net runoff out of the mascon over  $\Delta t$ , respectively. Based on eq (1), when precipitation exceeds runoff ( $\sum P - \sum R > 0$ ), any TWS drawdown (or negative  $\Delta TWS$ ) must be influenced by a change in storage due to ET. To determine if precipitation exceeds runoff during GRACE/FO-observed TWS drawdowns, we compared R estimates from a multi-forcing observation-based global runoff reanalysis (Ghiggi et al., 2021) to P estimates from the Global Precipitation Climatology Project (Gebremichael et al., 2003). We found that in nearly all ~~analyzed~~analysed mascon locations, the ~~cumulative sum of average~~  $P - R$  is positive during at least the five largest TWS drawdowns (Fig. A1), confirming these TWS drawdowns reflect root-zone water storage ~~consumed~~transpired by ecosystems and not loss of water in the mascon due to runoff.

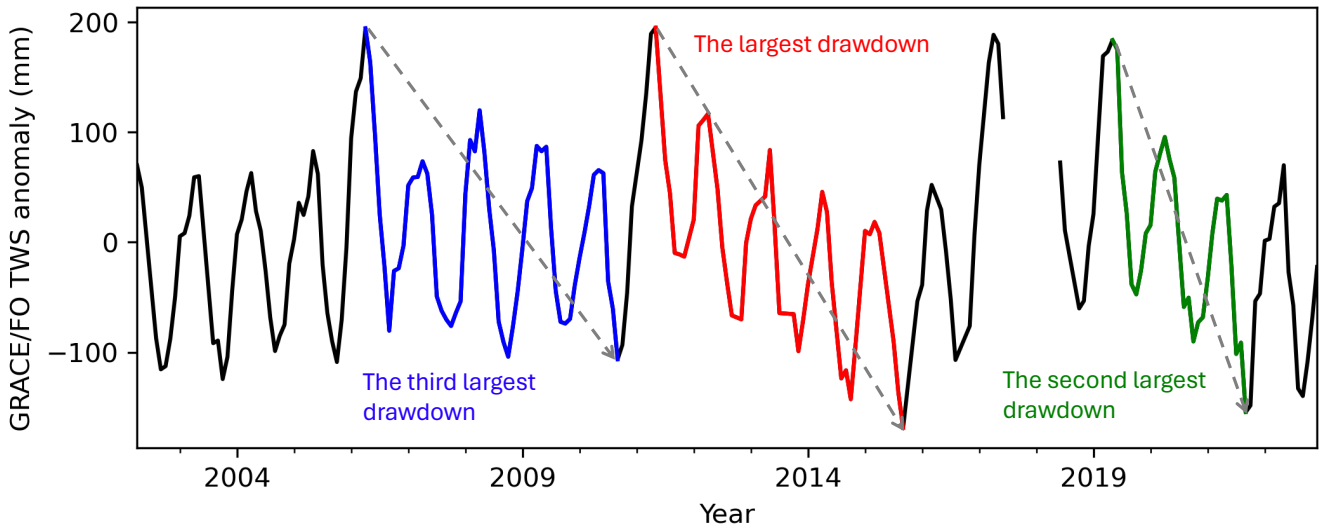


**Figure 1.** Example of TWS time series showing the three largest TWS-drawdowns at a mascon location in southern Idaho.

We estimated root-zone water storage capacity  $S_r$  to be the largest TWS drawdown during the record period of GRACE/FO (denoted as  $S_r^{GRACE/FO}$ ). To avoid overestimating  $S_r$ , we removed the impact of groundwater pumping, snow, and surface water on TWS drawdowns. Groundwater pumping, Anthropogenic groundwater use often manifested manifests as a negative long-term trend in the TWS time series (Rodell et al., 2018; Rodell et al., 2009; Feng et al., 2013). For example, regions showing significant TWS decreasing trends largely coincide with well-known groundwater irrigation areas identified in AQUASTAT data (Fig. A2), ~~is a human-made withdrawal of water resources.~~ To avoid conflating this drawdown with  $S_r$ , we first calculated the TWS trend by simultaneously fitting an annual and a ~~semiannual~~ semi-annual signal, a linear trend, and a constant to the GRACE/FO time series (Fig. A2). Then, we assumed any negative trend was attributable to groundwater pumping and removed the negative trend from the original GRACE/FO time series before calculating the TWS drawdowns. In high-latitude and mountainous regions, the maximum TWS anomaly during drawdowns may include snow. To avoid attributing snow storage to root-zone water storage, we first determined the largest drawdown from the full GRACE/FO time series and then calculated  $S_r$  using the maximum and minimum TWS anomaly with a monthly mean air temperature above 5°C. We obtained air temperature data from the fifth-generation European Centre for Medium-Range Weather Forecasts atmospheric reanalysis of the global climate (ERA5) (Hersbach et al., 2020). Following Wang et al. (2023) Wang et al. (2023a), we used total runoff from Ghiggi et al. (2021), which includes both surface runoff and subsurface runoff, as a proxy for surface water storage change (i.e.,  $\Delta SW = R$ ) and removed it from TWS drawdowns to isolate ~~the subsurface~~  $\Delta SW$  contributions (water stored in rivers, lakes, and reservoirs) to the GRACE/FO signal. This approach assumes that (1)  $R$  directly contributes to an increase in surface water levels within the drainage network, and (2) it takes approximately one month for  $R$  to exit the drainage system, aligning with the monthly time step of GRACE/FO data. Note that total runoff from Ghiggi et al. (2021)



109 stopped in 2019, and we used monthly climatology values between 2002 and 2019 to extend the data to 2022 and align with  
 110 the GRACE/FO record length. Other contributions to TWS drawdowns, such as changes in water intercepted by leaf and  
 111 branch surfaces and internal plant water storage, are too small to be detected by GRACE/FO (Rodell et al., 2005) and unlikely  
 112 to significantly affect our estimates. Our method also implicitly includes moisture stored in the topsoil for soil evaporation  
 113 (Stoy et al., 2019). However, the contribution of soil evaporation to ET decreases quickly as TWS draws down (Stocker et al.,  
 114 2023), and we expect that the magnitude of the largest drawdown will be determined by root-zone depletion magnitude  
 115 reflected at the end of the drawdown.

116 We calculated the random error of  $S_r^{GRACE/FO}$  by adding errors of the two GRACE/FO measurements and the  
 117 uncertainty of groundwater pumping and surface water signals in quadrature. To calculate the GRACE/FO measurement error,  
 118 we used the formal error product provided by the JPL mascon solutions (Watkins et al., 2015; Wiese et al., 2016). For the  
 119 uncertainty of groundwater pumping and surface water signals, we assumed a  $\pm 50\%$  error on the magnitude of our calculated  
 120 signals, following Zhao et al. (2021). This assumption implies that the uncertainty range is equal to the signals themselves,  
 121 leading to a likely conservative error estimate.

## 122 2.3 Comparison to other $S_r$ estimates

123 We compared our  $S_r^{GRACE/FO}$  estimate to two other  $S_r$  datasets. These datasets represent the typical rooting depth  $\times$  soil  
 124 texture-dependent water holding capacity approach (referred to as  $S_r^{RD \times WHC}$ ) and the water deficit accumulation approach  
 125 (referred to as  $S_r^{accum}$ ). We chose the  $S_r^{accum}$  estimate from Stocker et al. (2023) because it used the latest Earth observation-  
 126 constrained estimates of precipitation and evapotranspiration. We used their “ $S_{CWD \times 80}$ ” product which was estimated based on  
 127 cumulative water deficit extremes occurring with a return period of 80 years. We calculated  $S_r^{RD \times WHC}$  using existing datasets  
 128 on rooting depths and soil texture. The  $RD \times WHC$  approach requires knowing effective rooting depths (Federer et al., 2003;  
 129 Speich et al., 2018; Stocker et al., 2023; Bachofen et al., 2024). We obtained effective rooting depths from Yang et al. (2016),  
 130 who retrieved/derived them using an analytical model that balances the marginal carbon cost and benefits of deeper roots. Soil  
 131 water holding capacity While such model-based datasets are valuable for providing comprehensive coverage and insights into  
 132 complex processes, they do not incorporate direct observational data for validation or correction. Soil water holding capacity,  
 133 defined as the difference between field capacity and permanent wilting point, is calculated based on soil texture information  
 134 from the Harmonized World Soil Database version 1.2 (Wieder et al., 2014) and pedo-transfer functions based on Balland et  
 135 al. (2008). The Harmonized World Soil Database provides information for depths of 0-0.3 m and 0.3-1 m. For depths greater  
 136 than 1 m, we assume texture values from the 0.3-1 m depth following Stocker et al. (2023). For consistency, we spatially  
 137 averaged both  $S_r^{accum}$  and  $S_r^{RD \times WHC}$  estimates to match the GRACE/FO spatial scale ( $3^\circ \times 3^\circ$ ).

139 To evaluate the relative accuracy of  $S_r^{GRACE/FO}$ ,  $S_r^{accum}$ , and  $S_r^{RD \times WHC}$ , we used each of them to separately parameterize  
 140 a hydrologic model, labeled as  $HydroModel(S_r^{GRACE/FO})$ ,  $HydroModel(S_r^{accum})$ , and  $HydroModel(S_r^{RD \times WHC})$ , respectively. Then,  
 141 we compared the performance of the three models, assessed by their accuracy in simulating observations of TWS and ET. The  
 142 atmospheric forcing data and model parameters used in all simulations were identical except for  $S_r$ . Therefore, their relative  
 143 model performance demonstrates the differential accuracy between the three estimates. A monthly hydrologic model  
 144 developed by the United States Geological Survey (USGS) (Meece and Markstrom, 2007) was used due to its simplicity and  
 145 transparency about physical processes. Validating large-scale  $S_r$  remains inherently difficult because direct measurement of  $S_r$   
 146 is challenging. Previous studies have primarily employed two indirect methods: comparison to measured rooting depths and  
 147 hydrological modelling. Stocker et al. (2023) converted their deficit-based  $S_r$  estimates ( $\sim 5$  km resolution) into rooting depths  
 148 using soil texture and water-holding capacity parameters and then compared them to field rooting depth measurements  
 149 aggregated at biome levels to mitigate the scale mismatch. However, this approach is not suitable for our study as GRACE/FO-  
 150 derived  $S_r$  ( $\sim 300$  km) encompasses multiple biome types within the effective resolution of GRACE/FO data, making biome-  
 151 level aggregation less meaningful. Additionally, the rooting depth method overlooks groundwater and rock moisture  
 152 contributions to  $S_r$ , which Stocker et al. (2023) found to be significant in over half of their root measurement sites. This  
 153 omission will likely become more critical at the spatial scale of GRACE/FO, which averages larger areas and includes more  
 154 diverse biome types. These factors make the rooting depth comparison unsuitable for evaluating GRACE/FO-derived  $S_r$ .  
 155 Wang-Erlandsson et al. (2016) used deficit-based  $S_r$  estimates in a simple hydrological model and assessed improvements in  
 156 simulating hydrologic time series. While this approach better aligns with the scale of GRACE/FO, it is constrained by the  
 157 limited availability of high-quality global hydrologic data. This can lead to a circular use of the same data for both  $S_r$  estimation  
 158 and model evaluation, as seen when Wang-Erlandsson et al. (2016) used satellite-based ET data for both  $S_r$  estimation and  
 159 model evaluation, reducing the independence of the validation process. We also ~~Specifically, the model relies on a~~  
 160 ~~straightforward specification of  $S_r$  as a “water bucket” depth rather than indirectly through prescribed rooting depth, soil~~  
 161 ~~texture, and pedo-transfer functions across the profile. This allows us to parameterize the model directly with  $S_r^{GRACE/FO}$ ,  $S_r^{accum}$ ,~~  
 162 ~~and  $S_r^{RD \times WHC}$ . The USGS model was run at each GRACE mascon location with air temperature forcing from ERA5 and~~  
 163 ~~precipitation forcing from GPCP. We used climate forcing from 1993 to 2001 to spin up the model and performed water cycle~~  
 164 ~~simulations for the study period from 2002 to 2022. No calibrations were carried out.~~

165 We compared the performance between  $HydroModel(S_r^{GRACE/FO})$ ,  $HydroModel(S_r^{accum})$ , and  $HydroModel(S_r^{RD \times WHC})$   
 166 in capturing observed anomalies in TWS and ET. We opted for TWS anomalies as a comparison because they are directly  
 167 observable (by GRACE/FO) and are most relevant to the root-zone storage process. As the USGS model does not provide a  
 168 standard output variable for TWS, we used the sum of total root-zone water storage and surface snow amount as an  
 169 approximation of it, following previous studies (Jensen et al., 2019; Scanlon et al., 2018). Due to a lack of groundwater  
 170 compartment, the USGS model may underestimate large decadal declining and rising water storage trends relative to

GRACE/FO (Seanlon et al., 2018). To minimize this impact on our model comparison, we detrended both the GRACE/FO TWS time series and the model simulations of TWS. For consistency with GRACE/FO, modeled TWS anomalies were calculated by subtracting the time mean between 2002 and 2022 from the modeled TWS time series. Despite being the same dataset used in calculating  $S_r^{GRACE/FO}$ , using GRACE/FO as reference data is not circular because we calculated  $S_r^{GRACE/FO}$  by taking the difference of only two measurements (i.e., the maximum and minimum TWS values during the largest TWS drawdown). The complete GRACE/FO time series remains a useful dataset for evaluating model performance.

In addition, we compared model performance in simulating ET anomaly. We noted that existing gridded ET products generally have assumed ecosystem responses to water stress in their algorithms and are thus highly uncertain (Miralles et al., 2016). Most of these algorithms use so-called  $\beta$ -based formulations to model the impact of water stress on transpiration, reducing ET by a multiplicative stress factor  $\beta$  that depends on soil moisture (Trugman et al., 2018). These formulations contain errors and can have unknown impacts on the model performance evaluation (Tang et al., 2024; Miralles et al., 2016; Pascolini-Campbell et al., 2020). Instead, we used ET estimates derived from a water balance approach provided by Xiong et al. (2023). They calculated ET using eq (1) for major river basins by generating 4669 probabilistic unique combinations of 23 precipitation, 29 total runoff, and 7 water storage change datasets. These ET estimates are based on mass conservation and thus do not have assumed plant water relations. We only considered basins with an area extent larger than the nominal resolution of GRACE/FO ( $\sim 100,000 \text{ km}^2$ ). As the USGS hydrologic model was run at the mascon scale, we followed Zhao et al. (2022) to aggregate basin-scale modeled ET from mascon scale model outputs. We first identified all mascons that fully or partially cover a given basin and calculated the percentage of the total basin area covered by each mascon. We then used these percentage values as weights to calculate the basin-average ET from each mascon model output. Due to biases in existing precipitation and runoff datasets, the water balance-based ET estimates are also biased (Xiong et al., 2023; Rodell et al., 2004; Swenson and Wahr, 2006; Velicogna et al., 2012). These biases are challenging to correct, as unbiased global ET products are rare and almost non-existent (Miralles et al., 2016; Tang et al., 2024). To reduce its impact on our model evaluation, we focused on ET anomalies and calculated them by removing the corresponding temporal mean from both model output and water balance-based estimates following previous studies (Pascolini-Campbell et al., 2020; Velicogna et al., 2012).

The Nash-Sutcliffe model efficiency coefficient (NSE) To address these challenges, we evaluated the relative accuracy of  $S_r^{GRACE/FO}$ ,  $S_r^{accum}$  and  $S_r^{RD \times WHC}$  by separately parameterizing a hydrological model with each estimate, referred to as  $HydroModel(S_r^{GRACE/FO})$ ,  $HydroModel(S_r^{accum})$ , and  $HydroModel(S_r^{RD \times WHC})$ . We then assessed their accuracy in simulating ET using an independent dataset: version 4.1 of the Global Land Evaporation Amsterdam Model (GLEAM) ET (Miralles et al., 2024). This dataset was not involved in the calculation of  $S_r^{GRACE/FO}$ ,  $S_r^{accum}$ , or  $S_r^{RD \times WHC}$ , ensuring independence and avoiding circular validation that affected previous studies (e.g., Wang-Erlandsson et al., 2016). Furthermore, the GLEAM ET product provides several key improvements over other gridded ET products. For example, it combines hybrid learning from eddy-covariance and sap flow to better capture vegetation response to drought (Koppa et al., 2022) and explicitly accounts for plant access to groundwater (Hulsman et al., 2023). The atmospheric forcing data and model parameters were identical across

simulations, with  $S_r$  being the only variable parameter. Therefore, differences in model performance reflect the relative accuracy of the three  $S_r$  estimates. A monthly hydrologic model developed by the United States Geological Survey (USGS) (McCabe and Markstrom, 2007) was used due to its simplicity and transparency about physical processes. Specifically, the model relies on a straightforward specification of  $S_r$  as a “water bucket” depth rather than indirectly through prescribed rooting depth, soil texture, and pedo-transfer functions across the profile. This allows us to parameterize the model directly with  $S_r^{GRACE/FO}$ ,  $S_r^{accum}$ , and  $S_r^{RD \times WHC}$ . The USGS model was run at each GRACE mascon location with air temperature forcing from ERA5 and precipitation forcing from GPCP. We used climate forcing from 1993 to 2001 to spin up the model and performed water cycle simulations for the study period from 2002 to 2022. No calibrations were carried out.

To mitigate the impact of possible biases embedded in GLEAM ET, the forcing data, and those caused by model uncertainty (as the USGS model is uncalibrated), we used standardized ET anomalies (i.e., Z-scores) as the target of validation and focused on assessing whether  $S_r$  improves the temporal dynamics of ET simulations (i.e., seasonal and interannual variations) rather than the absolute values of ET. The Nash-Sutcliffe model efficiency (NSE) coefficient was used to assess the predictive skill of each USGS hydrologic model, which is defined as:

$$NSE = 1 - \frac{\sum_{t=1}^T (X_o^t - X_m^t)^2}{\sum_{t=1}^T (X_o^t - \bar{X}_o)^2} \quad (2)$$

where  $X$  represents ~~TWS anomaly or the standardized~~ ET anomaly,  $\bar{X}_o$  is the mean of observed  $X$ , and  $X_o^t$  and  $X_m^t$  are observed and modeled  $X$  at time  $t$ , respectively (Nash and Sutcliffe, 1970). An NSE value closer to 1 indicates a better model performance in simulating  $X$ . ~~An, while an~~ NSE value less than 0 indicates that the mean observed value is a better predictor than the simulated value, suggesting an unsatisfactory model performance (Nash and Sutcliffe, 1970). If  $HydroModel(S_r^{GRACE/FO})$ ,  $HydroModel(S_r^{accum})$ , and  $HydroModel(S_r^{RD \times WHC})$  all yield negative NSE values, the efficacy of using the USGS hydrologic model to evaluate the relative accuracy of the three  $S_r$  estimates is compromised. ~~Here, we focused on mascons and basins where at least one of the three models achieved a positive NSE value.~~

## 2.5 $S_r$ linkage to vegetation growth

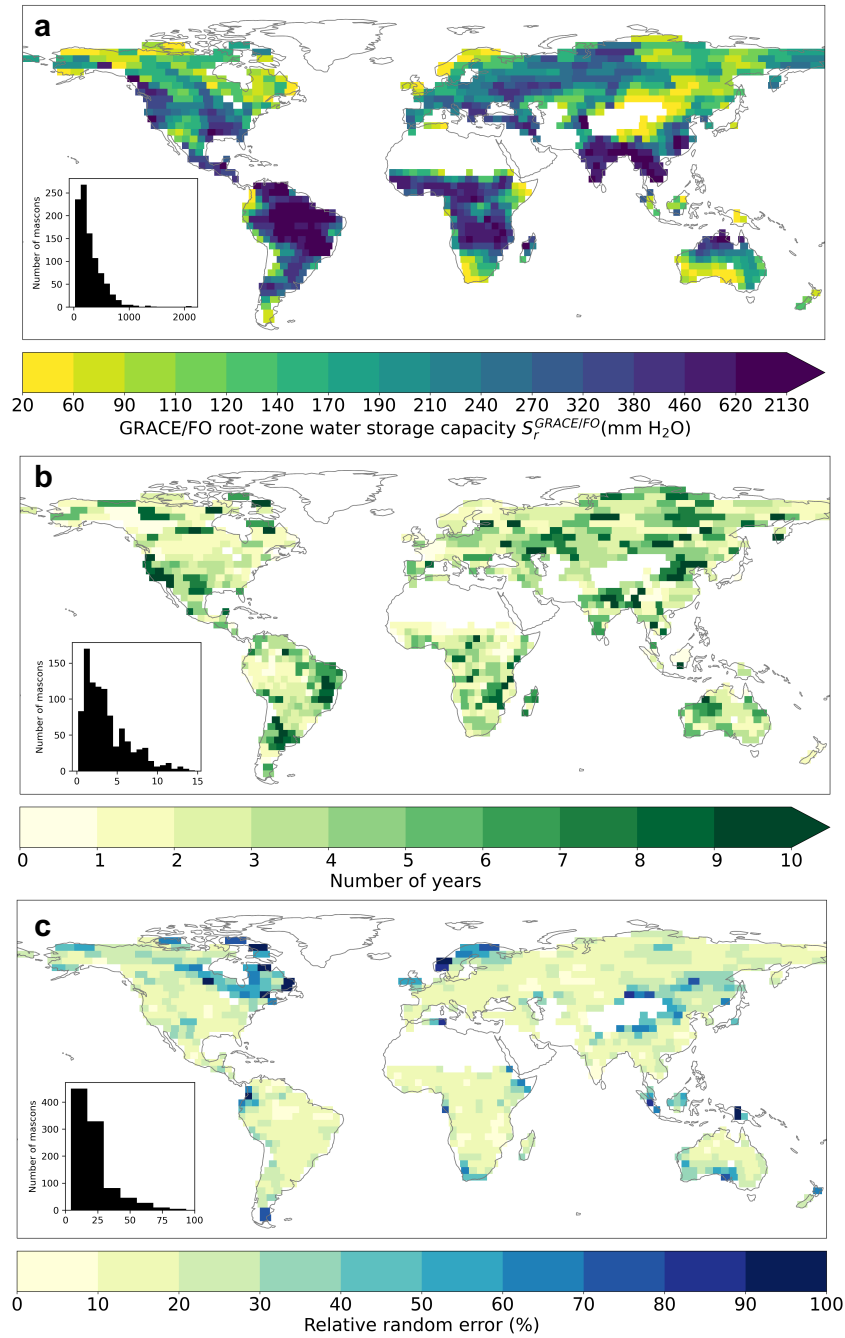
The  $S_r^{GRACE/FO}$  ~~is derived from the water balance, but its ecological relevance remains undetermined. To investigate whether  $S_r^{GRACE/FO}$  reflects vegetation water use for growth, we compared it with an independent measure of ecosystem productivity. We used maximum gross primary productivity ( $GPP_{max}$ ) to represent the potential GPP when the root zone is saturated with water. We obtained GPP data from the global MODIS and FLUXNET derived daily GPP product from 2000 to 2020 (Joiner and Yoshida, 2021). We chose this GPP product because it maximized the use of MODIS reflectance bands and demonstrated excellent validation results and agreement with other commonly used GPP products (Joiner and Yoshida, 2020).~~

## 231 **3 Materials and methods**

## 232 **3 Results**

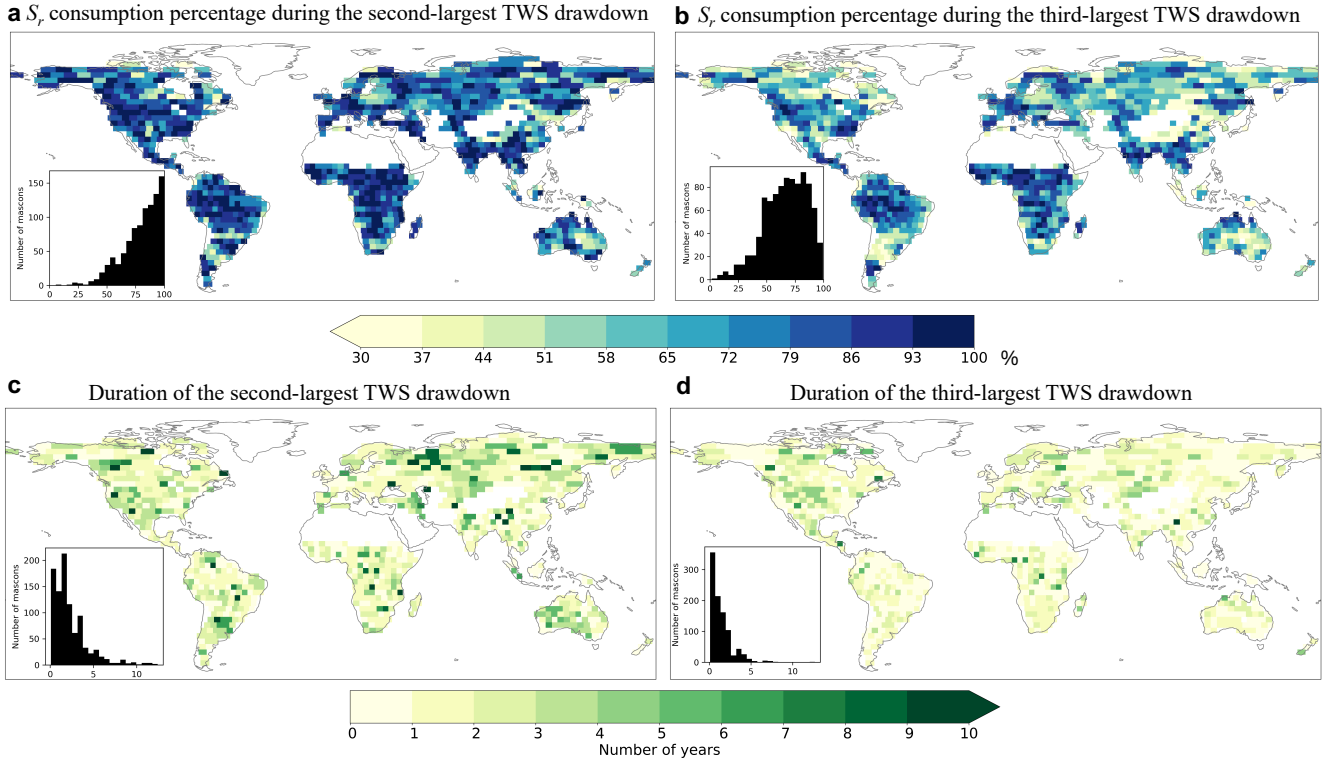
### 233 **3.1 $S_r$ from GRACE/FO ( $S_r^{GRACE/FO}$ )**

234 We find a substantial root-zone water storage capacity worldwide. Across the global vegetated domain,  $S_r^{GRACE/FO}$  (or  
235 the largest TWS drawdown) spans from 22 to 2131 mm (Fig. 2a). The distribution of  $S_r^{GRACE/FO}$  is positively skewed, with a  
236 median value of 221 mm (129 - 389 mm interquartile range; note that values in parentheses hereafter always refer to the  
237 interquartile range). Larger  $S_r^{GRACE/FO}$  ~~is~~are associated with densely vegetated regions like the tropical rainforests, the  
238 Southeastern U.S., the Pacific Northwest, and the southern part of China ~~while~~. By contrast, smaller  $S_r^{GRACE/FO}$  ~~is~~are found in  
239 sparsely vegetated regions like Central Asia, much of Australia, and some Arctic regions (Fig. 2a). Fig. 2b shows the duration  
240 of the maximum TWS drawdown with a global median of 2.8 years (1.6 - 5.2 years). We find no correlation between the  
241 duration and the magnitude of the largest TWS drawdown across different regions (Figs. 2a-b). The impact of random error  
242 sources on our  $S_r^{GRACE/FO}$  estimate remains moderate, with a global median relative error of 18% (13% - 26%) (Fig. 2c).



243  
 244 **Figure 2.**  $S_r$  estimated from GRACE/FO total water storage (TWS) anomaly. (a) Global patterns of  $S_r^{GRACE/FO}$  for Earth's  
 245 vegetated regions. (b) The duration of the maximum TWS drawdown. (c) Global patterns of the random error of  $S_r^{GRACE/FO}$ .  
 246 Insets in (a) - (c) show the histograms of corresponding mapping variables across our study area. White spaces on land represent  
 247 mascon locations with less than 50% vegetation cover.

248 To characterize the utilization of root-zone water storage capacity, we compared the second and third-largest TWS  
 249 drawdowns to  $S_r^{GRACE/FO}$ . We find that, on average, the second-largest TWS drawdown consumes 83% (71% - 92%) of the  
 250  $S_r^{GRACE/FO}$  estimate (Fig. 3a), while the third-largest uses 68% (54% - 82%) (Fig. 3b). The average duration of the second- and  
 251 third-largest TWS drawdowns decreases from 1.6 years (1.1 - 3.2 years) to 1.2 years (0.5 - 1.7 years) (Figs. 3c-d). In about  
 252 40% of our ~~analyzed~~ analysed mascons, the longest TWS drawdown period does not coincide with the largest drawdown  
 253 magnitude. These findings underscore the nuanced dynamics of water storage use within the root zone, suggesting variability  
 254 in both magnitude and duration across different regions.  
 255



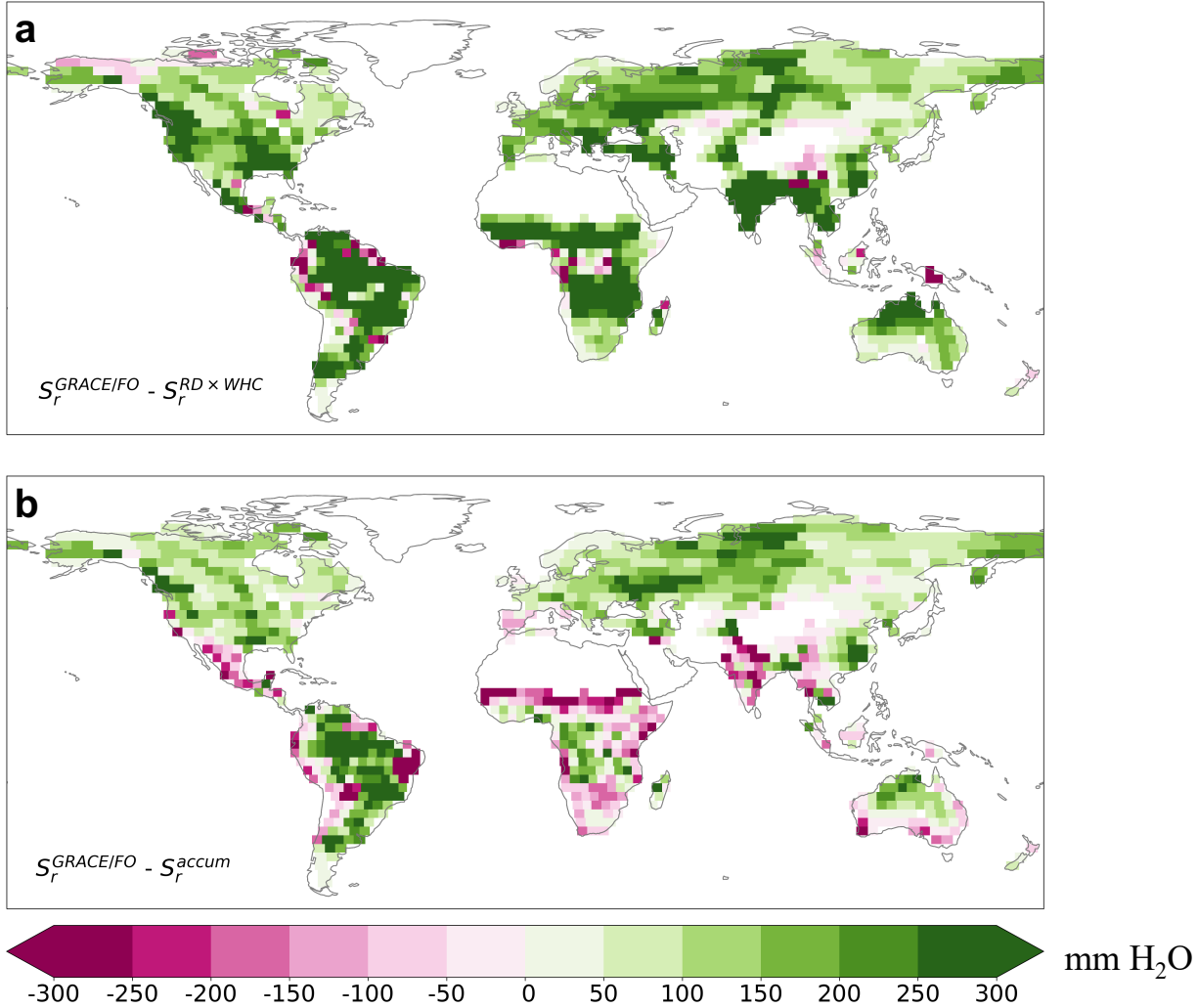
256  
 257 **Figure 3.** Utilization of root zone water storage capacity. (a) and (b) are the  $S_r^{GRACE/FO}$ -consumption percentages of  $S_r^{GRACE/FO}$   
 258 during the second and third-largest TWS drawdowns. (c) and (d) are the duration of the second and third-largest TWS  
 259 drawdowns. Insets in (a) - (d) show the histograms of corresponding mapped variables.

### 260 3.2 Comparison with other $S_r$ estimates

261 Our  $S_r^{GRACE/FO}$  estimate is larger than  $S_r^{RD \times WHC}$  and  $S_r^{accum}$  over much of the globe. Figs. 4a-b show  $S_r^{GRACE/FO}$  difference  
 262 with  $S_r^{RD \times WHC}$  and  $S_r^{accum}$ , respectively. Across the global vegetated domain,  $S_r^{GRACE/FO}$  surpasses  $S_r^{RD \times WHC}$  in over 90% of  
 263 mascon locations, with a median value 175 mm (or 380%) higher than that of  $S_r^{RD \times WHC}$ . The  $S_r^{GRACE/FO}$  exceeds  $S_r^{accum}$  over  
 264 70% of the study area, with a median value 77 mm (or 53%) higher than that of  $S_r^{accum}$ , despite exhibiting lower values in drier



265 ~~climates and lower biomass~~many regions of Africa, India, Mexico, and northeast Brazil (Fig. 4b). Notably, these differences  
 266 are greater than the random error of  $S_r^{GRACE/FO}$ , emphasizing that the underestimations by  $S_r^{RD \times WHC}$  and  $S_r^{accum}$  are significant.



267 -300 -250 -200 -150 -100 -50 0 50 100 150 200 250 300 mm H<sub>2</sub>O  
 268 **Figure 4.**  $S_r^{GRACE/FO}$  ~~comparison with~~is notably larger than other datasets over much of the globe. (a) The difference between  
 269  $S_r^{GRACE/FO}$  and  $S_r^{RD \times WHC}$ . (b) The difference between  $S_r^{GRACE/FO}$  and  $S_r^{accum}$ .

### 270 3.3 Implementation in the USGS hydrologic model

271 To assess whether  $S_r^{GRACE/FO}$  is an improvement over  $S_r^{accum}$  and  $S_r^{RD \times WHC}$ , we used each of them to separately  
 272 parameterize the USGS hydrologic model. We first evaluated the accuracy of  $HydroModel(S_r^{GRACE/FO})$ ,  $HydroModel(S_r^{RD \times WHC})$ ,  
 273 and  $HydroModel(S_r^{accum})$  in replicating the full time series of standardized GLEAM ET anomalies. For over 95% of the global  
 274 vegetated domain, at least one model achieved a positive NSE value. In these regions, the average NSE for  
 275  $HydroModel(S_r^{GRACE/FO})$  is 0.73 (0.65 - 0.89), for  $HydroModel(S_r^{RD \times WHC})$  it is 0.69 (0.63 - 0.86), for  $HydroModel(S_r^{accum})$  it is

0.72 (0.64 - 0.87). These relatively high NSE values indicate the USGS model is effective in simulating ET. While the global average NSE values for the three models are similar,  $HydroModel(S_r^{GRACE/FO})$  demonstrates slightly superior performance, outperforming  $HydroModel(S_r^{RD \times WHC})$  in 66% of the vegetated regions and  $HydroModel(S_r^{accum})$  in 59% of these regions (Fig. 5). time series of GRACE/FO TWS anomalies. No model attains positive NSE values for approximately 40% of the global vegetated domain (Fig. A3), suggesting the USGS model may not effectively discern the relative accuracy of the three  $S_r$  estimates at these locations. However, for the remaining 60%;

We hypothesized that a more accurate  $S_r$  would have a greater impact on improving ET simulations during drought periods when ET is more dependent on deep subsurface water storage. To test this, we calculated NSE values specifically for drought periods, defined as when the 3-month standardized precipitation index was less than -1.2, indicative of severe drought conditions (McKee et al., 1993). Across 87% of the global vegetated domain, at least one model achieved a positive NSE value. In these regions, the average NSE for  $HydroModel(S_r^{GRACE/FO})$  is 0.39 (0.23 - 0.59), for  $HydroModel(S_r^{RD \times WHC})$  it is -9.33 (-26.66 - 0.30), for  $HydroModel(S_r^{accum})$  it is -0.22 (-0.09 - 0.56). The  $HydroModel(S_r^{GRACE/FO})$  outperformed  $HydroModel(S_r^{RD \times WHC})$  in terms of NSE values across 89% of these regions and outperformed  $HydroModel(S_r^{accum})$  across 67% of these regions (Fig. 6) (0.52 - 0.86), for  $HydroModel(S_r^{RD \times WHC})$  it is 0.52 (0.40 - 0.81), for  $HydroModel(S_r^{accum})$  it is 0.61 (0.48 - 0.84). These lower NSE values compared to the full ET time series reflect the challenges faced by the USGS model in simulating ET during droughts, consistent with previous findings (e.g., Zhao et al., 2022). However,  $HydroModel(S_r^{GRACE/FO})$  showed notable improvement over the other two models, particularly in high-latitude regions (Fig. 6). These results suggest that while  $S_r^{GRACE/FO}$  provides only marginal improvements for the full time series of standardized GLEAM ET anomalies, its superiority over  $S_r^{RD \times WHC}$  and  $S_r^{accum}$  becomes more pronounced during drought conditions. 5). For example, at a wet mascon location in the Pacific Northwest (Fig. 6a), the NSE values for  $HydroModel(S_r^{GRACE/FO})$ ,  $HydroModel(S_r^{RD \times WHC})$ , and  $HydroModel(S_r^{accum})$  are 0.68, -3.69, and 0.42, respectively (Fig. 6b). For a dry mascon in Mexico (Fig. 6a), the NSE values for  $HydroModel(S_r^{GRACE/FO})$ ,  $HydroModel(S_r^{RD \times WHC})$ , and  $HydroModel(S_r^{accum})$  are 0.64, -45.6, and 0.54, respectively (Fig. 6c). These results suggest an improved performance in simulating TWS temporal dynamics when parameterizing root-zone water storage capacity using  $S_r^{GRACE/FO}$  in the hydrologic model. Nevertheless,  $HydroModel(S_r^{accum})$  demonstrates superior performance in some drier climates and lower biomass regions. For instance, at a mascon in the Horn of Africa (Fig. 6a), the NSE value of  $HydroModel(S_r^{accum})$  is 0.46, significantly higher than that of  $HydroModel(S_r^{GRACE/FO})$  and  $HydroModel(S_r^{RD \times WHC})$ , which are -1.4 and -2.1, respectively (Fig. 6d). The comparison between Fig. 4b and Fig. 5b reveals that the underperformance of  $HydroModel(S_r^{GRACE/FO})$  compared to  $HydroModel(S_r^{accum})$  is associated with  $S_r^{GRACE/FO}$  consistently being lower than  $S_r^{accum}$  in these arid regions.

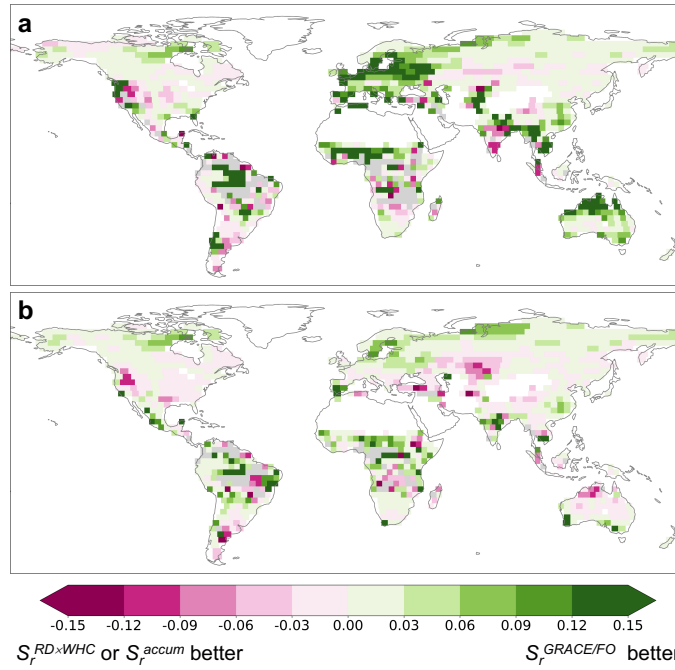
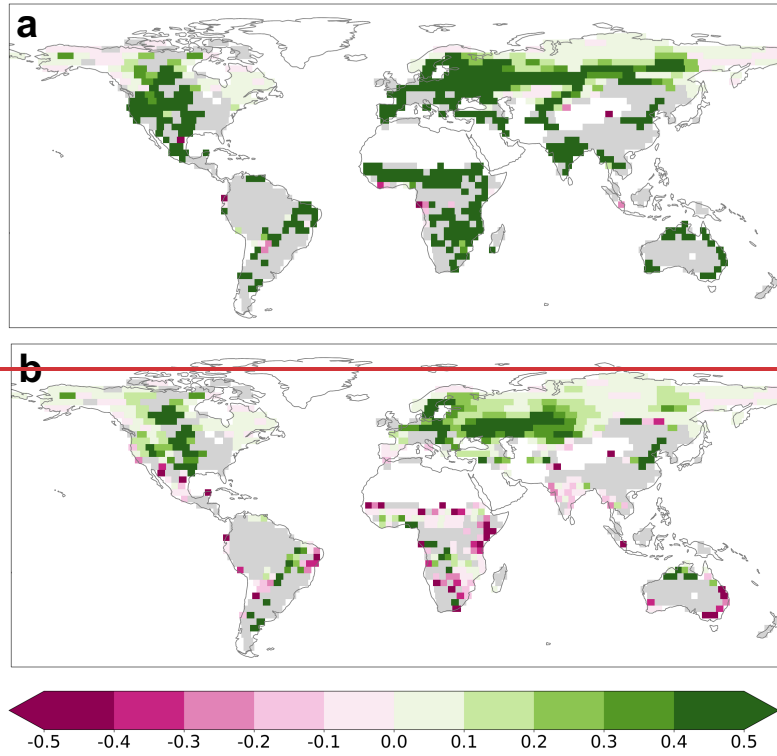
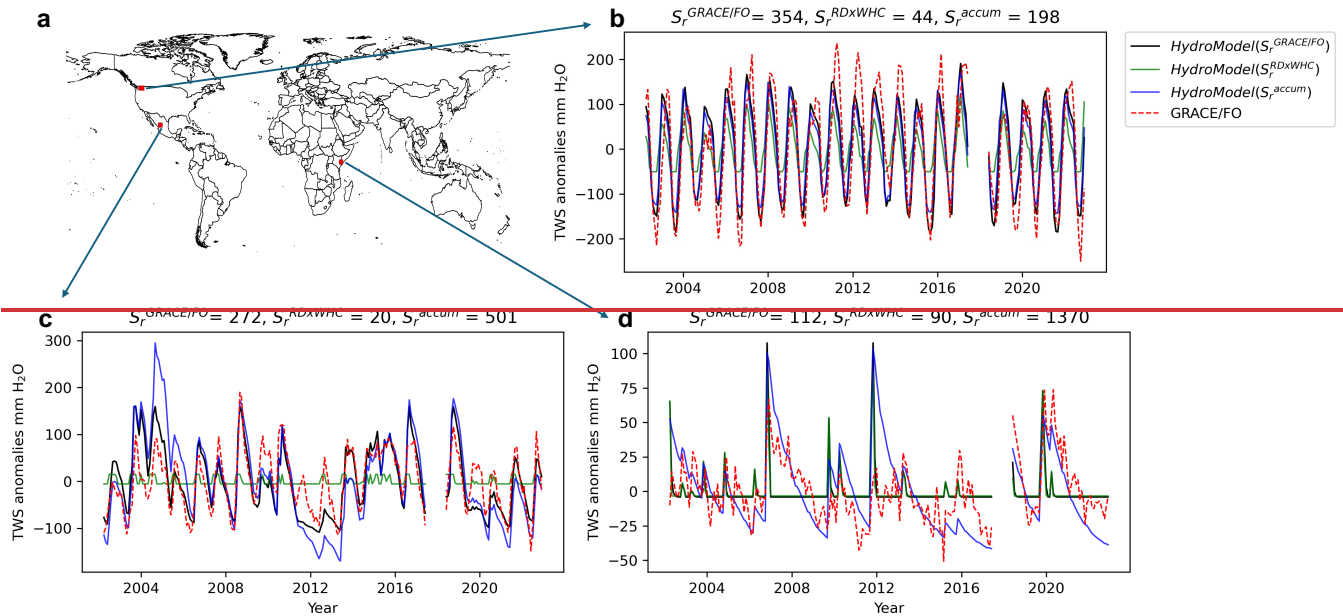
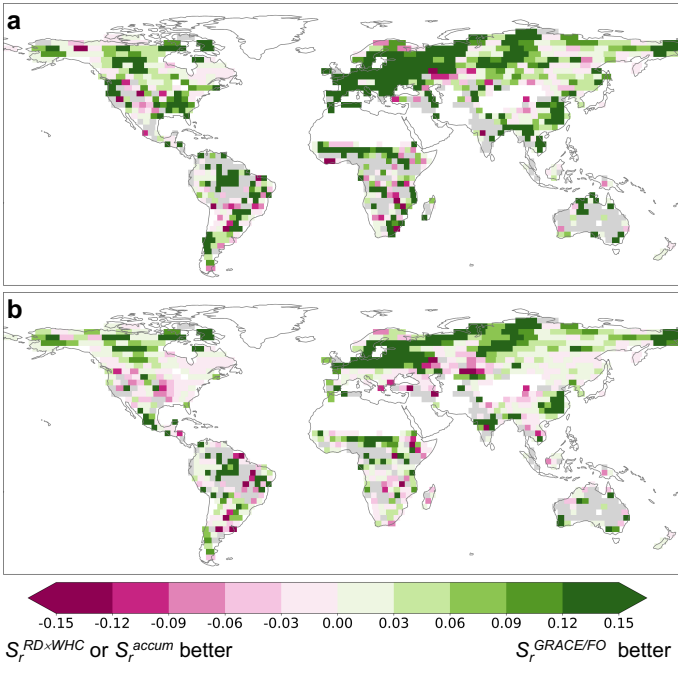


**Figure 5. Predictive skill differences for TWS anomalies.**  $S_r^{GRACE/FO}$  improves overall model performance in simulating standardized ET anomalies over much of the globe. (a) The NSE difference between  $HydroModel(S_r^{GRACE/FO})$  and

309  $HydroModel(S_r^{RDxWHC})$  for full time series. (b) The NSE difference between  $HydroModel(S_r^{GRACE/FO})$  and  
 310  $HydroModel(S_r^{accum})$ . The gray colors indicate areas where all models fail to achieve a  
 311 positive NSE value.  
 312



313



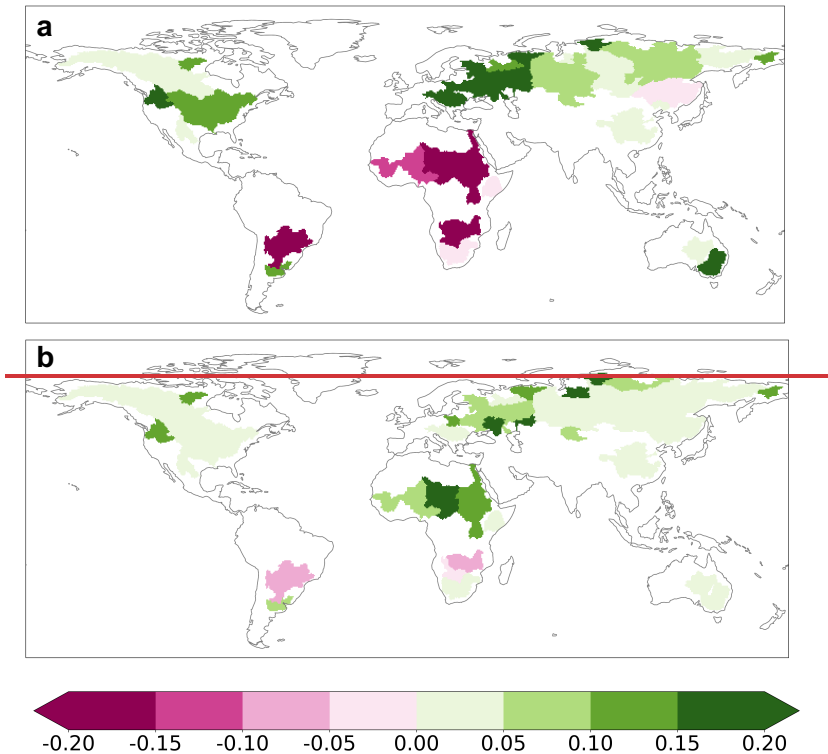
314

315 **Figure 6.** Time series comparison between GRACE/FO TWS and model simulations. (a) Location map of the three exemplary  
 316 maseons in the Pacific Northwest (b), Mexico (c), and the Horn of Africa (d). The values of  $S_r^{GRACE/FO}$ ,  $S_r^{RD \times WHC}$ , and  $S_r^{accum}$   
 317 are annotated on top of (b)–(d).

318  
 319 ——— In addition, we evaluated each model’s accuracy in simulating the time series of ET anomalies. The results show that  
 320 at least one model achieves a positive NSE value in 48 large river basins (Fig. 7). In these basins, the average NSE for  
 321  $HydroModel(S_r^{GRACE/FO})$  is 0.35 (0.13–0.63), for  $HydroModel(S_r^{RD \times WHC})$  it is 0.30 (0.10–0.54), and for  $HydroModel(S_r^{accum})$   
 322 it is 0.29 (0.06–0.58). Specifically,  $HydroModel(S_r^{GRACE/FO})$  outperformed  $HydroModel(S_r^{RD \times WHC})$  in terms of NSE values  
 323 across 37 basins and outperformed  $HydroModel(S_r^{accum})$  across 45 basins (Fig. 7).

324 Taken together, despite an absence of direct root zone storage measurements at scale,  $S_r^{GRACE/FO}$  notably improves  
 325 upon the water deficit based estimate and the rooting depth based estimate and reveals a substantially larger root zone storage  
 326 capacity across much of the globe. The improved simulation accuracy of TWS and model performance in simulating  
 327 standardized ET anomalies using  $S_r^{GRACE/FO}$  demonstrates the importance during drought periods across much of accurate  $S_r$   
 328 estimates for hydrological modeling.

329



330  
 331 **Figure 7.** Predictive skill differences for basin ET anomalies, the globe. (a) The NSE difference between  
 332  $HydroModel(S_r^{GRACE/FO})$  and  $HydroModel(S_r^{RD \times WHC})$ . (b) The NSE difference between  $HydroModel(S_r^{GRACE/FO})$  and

333 *HydroModel*( $S_r^{accum}$ ). White spaces on land represent basins where no model achieves a positive NSE value or no ET data is  
334 available.

### 335 3.4 Linking $S_r$ to vegetation growth

336 We evaluated the relationship between  $S_r^{GRACE/FO}$  and  $GPP_{max}$  to link root zone water storage capacity to vegetation  
337 growth. We observed a consistent increase in  $S_r^{GRACE/FO}$  alongside  $GPP_{max}$  across space (Fig. 8a). This trend reflects the intrinsic  
338 relationship between vegetation productivity and water supply across space (Huxman et al., 2004; Ponce Campos et al., 2013;  
339 Hsu et al., 2012). However, we noted a saturation effect at higher  $S_r^{GRACE/FO}$  values, suggesting a diminishing influence of water  
340 supply beyond a certain threshold. This aligns with ecological principles, particularly in wetter regions, where factors such as  
341 nutrient availability and light intensity may dominate over water availability in constraining  $GPP_{max}$  (Huxman et al., 2004;  
342 Ponce Campos et al., 2013; Hsu et al., 2012). Notably, since our  $S_r^{GRACE/FO}$  estimate is based on the water balance and does  
343 not rely on assumed plant water relations, this evidence supports the reliability of  $S_r^{GRACE/FO}$  and sheds light on the intricate  
344 interplay of environmental factors influencing vegetation dynamics across landscapes.

345 We also evaluated the  $S_r$  relationship with  $GPP_{max}$  using  $S_r^{RD \times WHC}$  and  $S_r^{accum}$  (Figs. 8b-c), finding that the overall  
346 pattern of the functional relationships is are similar to that observed using  $S_r^{GRACE/FO}$ . Specifically, the  $GPP_{max}$  increases with  
347 increasing  $S_r$  before reaching a plateau or showing a notably smaller change with further increases in  $S_r$ . However, the  
348 thresholds at which this apparent saturation occurs differ: approximately 400 mm for  $S_r^{GRACE/FO}$ , 50 mm for  $S_r^{RD \times WHC}$ , and 150  
349 mm for  $S_r^{accum}$ . To better understand the appropriate threshold, we compared our observed patterns to those inferred from the  
350 spatiotemporal origin of transpiration estimated by Miguez Macho and Fan (2021). They used inverse modeling and isotopic  
351 analysis to map the annual contribution of root zone water storage (or total past precipitation) to transpiration on a global scale.  
352 By multiplying their root zone water storage contribution with simulated transpiration, we derived a lower bound  $S_r$  estimate  
353 and compared it to annual transpiration across regions (Fig. 8d). Given the widely reported linear relationship between  
354 transpiration and vegetation growth across regions (Ponce Campos et al., 2013; Biederman et al., 2016; Cooley et al., 2022),  
355 Fig. 8d indicates that the deceleration in vegetation growth may occur at a lower bound  $S_r$  value of 400 mm. As  $S_r$  increases  
356 with higher lower bound  $S_r$  (due to their positive correlations with vegetation growth; Figs. 8a-c vs. 8d), the  $S_r$  threshold could  
357 exceed the 400 mm inferred from the lower bound  $S_r$  estimate. This aligns better with the threshold inferred from  $S_r^{GRACE/FO}$   
358 but is significantly higher than those inferred from  $S_r^{RD \times WHC}$  and  $S_r^{accum}$ . Therefore,  $S_r^{GRACE/FO}$  likely provides a more accurate  
359 reflection of real-world spatial patterns of land water supply on vegetation growth than  $S_r^{RD \times WHC}$  and  $S_r^{accum}$ .

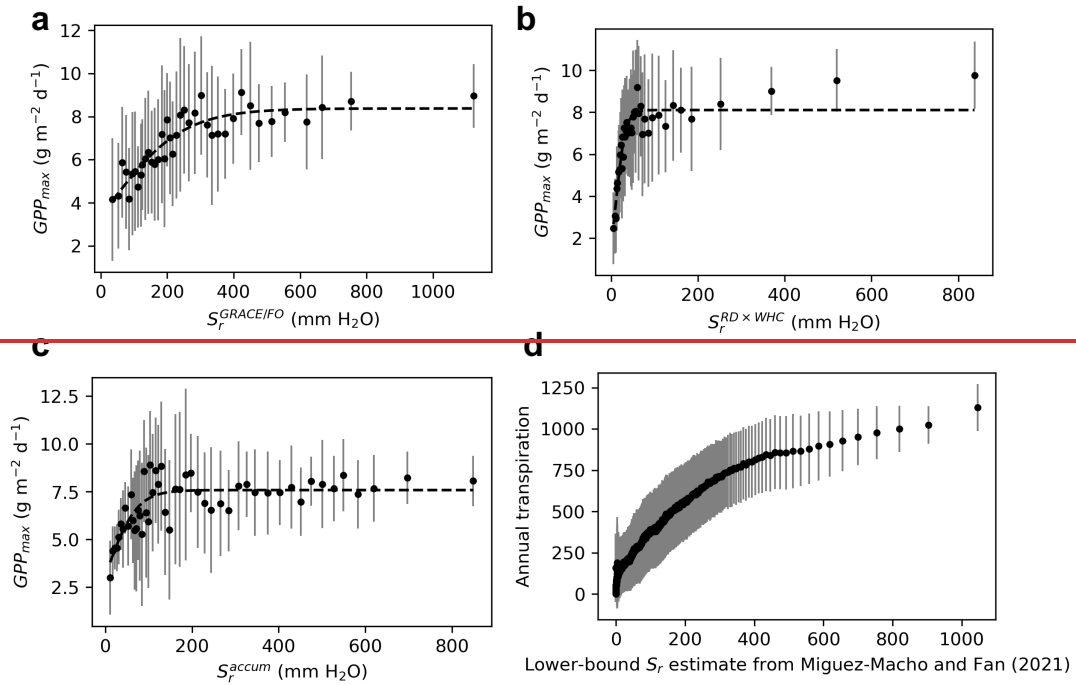


**Figure 8.** Scatterplots of  $GPP_{max}$  and  $S_r$  across regions based on  $S_r^{GRACE/FO}$  (a),  $S_r^{RD \times WHC}$  (b), and  $S_r^{accum}$  (c). All analyzed maseons are grouped into 40 equal-sized bins based on  $S_r$ . Circle and error bar denote the mean and standard deviation of  $GPP_{max}$  within each bin (Figs. 5a and 5b, respectively). The dashed black line in each plot represents a model fit using a nonlinear concave-down model. (d) is the lower-bound estimate of  $S_r$  derived from Miguez-Macho and Fan (2021) in relation to their simulated annual transpiration. Due to the high resolution of their inverse modeling ( $30'$ ), model grid-cells are grouped into 1000 equal-sized bins based on the lower-bound estimate of  $S_r$ . Circle and error bar denote the mean and standard deviation of annual transpiration within each bin, except for drought time periods. Gray areas indicate regions where all models fail to achieve a positive NSE value.

## 4 Discussion

### 4.1 Limitations and uncertainty in $S_r^{GRACE/FO}$

Our  $S_r^{GRACE/FO}$  estimate provides a conservative lower bound on  $S_r$  because the largest TWS drawdown during the GRACE/FO record period may not cover a period during which ET from storage exhausts the entire root-zone water storage capacity, particularly in areas experiencing water accumulation in the root zone due to increased increases in precipitation. This likely explains why our  $S_r^{GRACE/FO}$  estimate is lower than  $S_r^{accum}$  in North and East Africa, where strong increasing TWS trends were observed (Fig. 3b and Fig. A2) in response to increasing precipitation trends (e.g., Rodell et al., 2018). Additionally, our approach to account for groundwater pumping and surface water may overestimate these signals' actual magnitudes and thus likely contribute to underestimating  $S_r$ . Specifically, we assumed all negative TWS trends to be caused by groundwater



~~withdrawal~~withdrawals and removed them from  $S_r^{GRACE/FO}$ . However, intense groundwater ~~withdrawal is~~withdrawals are concentrated in specific regions such as northwest India, California's Central Valley, and the North China Plain (Rodell et al., 2009; Feng et al., 2013; Liu et al., 2022). Consequently, we may ~~remove~~have removed TWS depletion trends caused by natural variability, as seen in the drought-stricken Southeast Brazil (Rodell et al., 2018). This likely explains why  $S_r^{GRACE/FO}$  is lower than  $S_r^{accum}$  there (Fig. 3b). Furthermore, we used total runoff (which includes surface runoff, snowmelt, and groundwater ~~flow~~discharge) as a proxy to remove surface water storage change from the TWS drawdown. We used total runoff – as opposed to surface runoff alone (Wang et al., 2023) – ~~due to observational data availability, though doing so may lead to an overestimation of surface water storage change and, therefore, an underestimation of  $S_r$ .~~ (Wang et al., 2023a) – due to observational data availability, though doing so may lead to an overestimation of surface water storage change and, therefore, an underestimation of  $S_r$ .

#### 4.2 Multi-year drawdowns in $S_r^{GRACE/FO}$ and differences with $S_r^{accum}$

Despite being conservative,  $S_r^{GRACE/FO}$  reveals a substantially larger volume of root-zone water storage capacity than  $S_r^{accum}$ . One reason for this discrepancy may be the lack of interannual storage variability considered in the  $S_r^{accum}$  calculation (Stocker et al., 2023). Although Stocker et al. (2023) used a cumulative water deficit approach to infer root-zone water storage drawdown, akin to our TWS drawdown approach, they found that the annual totals of P exceeded those of ET at almost all locations. Because their method resets the calculation whenever accumulated P-ET is positive, this suggests their method generally was unable to account for carryover storage and multiyear drawdowns of root-zone storage. Our use of GRACE/FO TWS, which allows for multiyear drawdowns, is supported by recent observations (Goulden and Bales, 2019; MeeormiekMcCormick et al., 2021; Pérez-Ruiz et al., 2022; Peterson et al., 2021; Scott and Biederman, 2019) and ~~modeling~~modelling efforts (Miguez-Macho and Fan, 2021; Livneh and Hoerling, 2016) suggesting widespread carryover storage effects. Our calculations of  $S_r^{GRACE/FO}$  found that the largest TWS drawdown period lasted a median of 2.8 years, with an interquartile range between 1.6 and 5.2 years (Fig. 2c). Even the second and third-largest TWS drawdowns had a median duration of more than one year globally (Figs. 3c-d). These findings align with the results reported in the previously referenced studies on carryover storage effects.

#### 4.3 Groundwater and rock moisture in $S_r^{GRACE/FO}$ and differences with $S_r^{RD \times WHC}$

The  $S_r^{RD \times WHC}$  estimate notably falls below both  $S_r^{GRACE/FO}$  and  $S_r^{accum}$ . This discrepancy may be attributed to the  $RD \times WHC$  approach ignoring plant access to ~~bedrock~~moisture stored beneath the soil, such as in weathered and fractured bedrock and groundwater, ~~which. These deep moisture sources~~ are known to significantly affect ET and thus contribute to  $S_r$  (e.g., Fan et al., 2017; Rempe and Dietrich, 2018; MeeormiekMcCormick et al., 2021). ~~Moreover, the  $RD \times WHC$  approach lacks consideration for root density and its vertical and lateral distribution, simplifying the root zone's complexity. Unlike  $S_r^{RD \times WHC}$ , the definitions of  $S_r^{GRACE/FO}$  and  $S_r^{accum}$  incorporate natural variability in these deep moisture reserves, broadening the~~

traditional “root zone” concept beyond the unsaturated soil layer. This expanded definition acknowledges the dynamic nature of the root zone, with plants accessing deep groundwater and rock moisture during prolonged droughts and periods of high transpiration demand (Gao et al., 2024). Indeed, root-accessible water does not require roots to physically occupy the entire storage domain. Processes like capillary rise can move deep water upward to the traditional “root zone” for vegetation transpiration, especially during dry seasons and droughts.

The importance of including groundwater and rock moisture in  $S_r$  is well-supported by recent evidence. Studies using *in situ* groundwater (Fan et al., 2017; Thompson et al., 2011; Baldocchi et al., 2021; Li et al., 2015), remote sensing observations (Koirala et al., 2017; Rohde et al., 2024), and modeling efforts (Miguez-Macho and Fan, 2021; Hain et al., 2015) have demonstrated that plants can access these deep moisture sources and highlighted their critical role in sustaining ET, especially during extreme droughts. In many ecosystems, water stress can stimulate root growth into deep subsurface through the capillary rise effect, with roots extending to the capillary fringe and the water table, as observed in both field and laboratory studies (Naumburg et al., 2005; Orellana et al., 2012; Fan et al., 2017; Kuzyakov and Razavi, 2019). Although individual shallow-rooted plants (e.g., grassland sites) may not directly tap into groundwater or rock moisture, the large spatial scale of GRACE/FO likely captures water uptake across diverse vegetation types. Even in areas primarily covered by shallow-rooted vegetation, deeper-rooted plants within the same GRACE/FO mascon may redistribute water upward through hydraulic redistribution, making it available for shallow-rooted plants to use (e.g., Espeleta et al., 2004; Orellana et al., 2012). In fact, satellite observations have confirmed widespread plant-groundwater interactions at large spatial scales (Koirala et al., 2017), even in dryland regions dominated by grasslands (Rohde et al., 2024; Wang et al., 2023b). Recognizing and incorporating groundwater and bedrock moisture in root zone storage capacity can enhance our understanding of land-atmosphere interactions (Maxwell and Condon, 2016; Schlemmer et al., 2018; Dong et al., 2022), improve runoff simulations (Hahm et al., 2019), and provide a more accurate representation of vegetation resilience to droughts and heat waves (Jiménez-Rodríguez et al., 2022; Esteban et al., 2021).

The  $RD \times WHC$  approach, while useful for simplifying root zone complexity, overlooks critical aspects of root density, its vertical and lateral distribution, and the ability of plants to access deep water stores – factors that have significant implications for understanding ecosystem water uptake and improving land models. For instance, this approach reduces the complexity of rooting systems into a single effective rooting depth parameter (Federer et al., 2003; Speich et al., 2018). ~~This parameter, which~~ tends to be shallower than both the maximum rooting depth (Federer et al., 2003) and the depth that contains the upper 95% of the root biomass (Yang et al., 2016), ~~although these depths may~~. ~~These deeper layers, however, often~~ play a disproportionately important role in ecosystem water uptake (Fan et al., 2017; Jackson et al., 1999; Bachofen et al., 2024). Additionally, when dividing  $S_r^{GRACE/FO}$  with the same  $WHC$  used in  $S_r^{RD \times WHC}$  to calculate effective rooting depth, this depth exceeds 2 m in nearly 50% of global vegetated areas, in contrast to Yang et al.’s (2016) estimate of 10% and Stocker et al.’s (2023) estimate of 37%. ~~These results suggest that the potential for plants to tap into deep water stores is more prevalent than previously understood.~~ These results indicate that the potential for plants to tap into deep water stores is more prevalent than previously understood. For land models that do not explicitly incorporate  $S_r$  as a variable, this suggests that models with a soil

depth of less than 2 m (e.g., the Noah model within the Global Land Data Assimilation System (GLDAS)) may be unable to accurately simulate these deeper water drawdowns. Consequently, this limitation could impact studies of groundwater that rely on GLDAS to separate soil moisture from TWS (e.g., Rodell et al., 2009).

Despite different  $S_r$  parameterizations, the USGS hydrological model performs poorly in extremely wet and dry regions, such as the Amazon rainforest and much of Australia (Fig. A3), likely due to a lack of calibration of other parameters or an overly simplistic representation of key hydrological processes. The model's algorithm aims to meet the potential ET (PET), or the atmospheric demand for water, using precipitation and withdrawals from root zone water storage (Meece and Markstrom, 2007). It uses the Hamon equation (Hamon, 1964) to calculate PET, and previous studies (e.g., Sun et al., 2008; Meece et al., 2015) have found that the Hamon coefficient needs to be calibrated to generate realistic ET. However, calibrating the Hamon coefficient could absorb or compensate for the  $S_r$  parameterization error, undermining the objectiveness of the USGS model in evaluating the relative accuracy of the three  $S_r$  estimates. In very wet regions, the USGS model often simulates the PET significantly lower than incoming precipitation (Fig. A4). Consequently, the model does not need to tap root zone water storage for ET, resulting in little variability in TWS for these regions (Fig. A4). Conversely, in very dry regions, the USGS model simulates the PET to be notably higher than incoming precipitation most of the time, leaving the root zone water storage close to zero (Fig. A5). However, large variability in TWS was observed by GRACE/FO for these regions, which is consistent with other studies indicating strong soil moisture variations (Swann and Koven, 2017; Chen et al., 2014). These results suggest that structural errors or uncertainty of other parameters in the USGS model may outweigh the uncertainty of  $S_r$  parameterization in these very wet and dry environments.

~~This paper demonstrates how GRACE/FO data can be used to constrain vegetation water use patterns. Although observed at a coarse resolution, the  $S_r^{GRACE/FO}$  can be used to evaluate high-resolution  $S_r$  estimates to ensure consistency and accuracy across different scales. In addition~~**4.4 Strengths and limitations of  $S_r^{GRACE/FO}$  validation**

Although direct observations of  $S_r$  at large spatial scales are limited, our validation effort for  $S_r^{GRACE/FO}$  shows two notable strengths. First, we used an independent dataset for the validation of USGS models parameterized by different  $S_r$  estimates, unlike a previous study (Wang-Erlandsson et al., 2016), which relied on a dataset already used in their  $S_r$  calculation. Second, the GLEAM ET dataset used here for validation addresses key limitations of other gridded ET products by using a data-driven embedding of plant-water relationships (rather than explicitly assuming these a priori as most ET products do) and explicitly accounting for groundwater contributions to ET (Miralles et al., 2024).

Despite these strengths, our validation effort is not without limitations. First, the mechanistic linkage between  $S_r$  and commonly used hydrological indicators (e.g., ET and streamflow) is complex. Identifying decisive indicators that are highly sensitive to  $S_r$  is an ongoing research challenge. In this context, our findings provide an initial step towards understanding this relationship, demonstrating that a more accurate  $S_r$  improves simulations of drought-time ET anomalies more effectively than all-time variations (Figs. 5 and 6). However, resolving such a complex relationship is further complicated by model structural errors or uncertainties in other model parameters, which can obscure the true impact of accurate  $S_r$  parameterization on

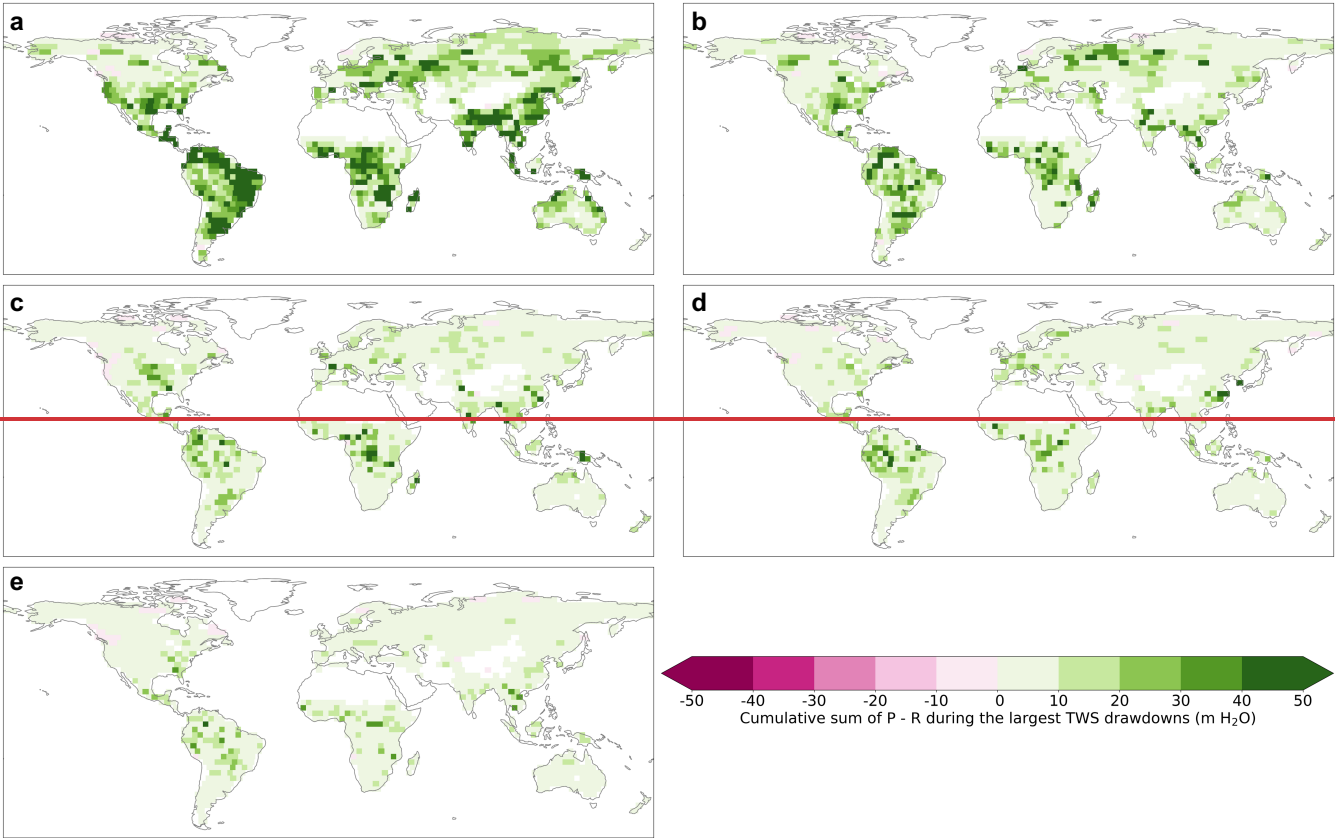
ecohydrological processes. For example, in our study, streamflow simulated by the USGS model is mainly driven by precipitation and shows limited sensitivity to  $S_r$  (results not shown). This aligns with the findings of another simple hydrologic model used by Wang-Erlandsson et al. (2016), as discussed in their open peer review file, where streamflow measurements were also not used for model evaluation. Second, we used standardized ET anomalies (Z-scores) as the validation target, focusing on temporal dynamics such as seasonal and interannual variations rather than absolute ET values. While this approach effectively mitigates the impact of data biases and ensures consistency, it narrows the scope of the validation.

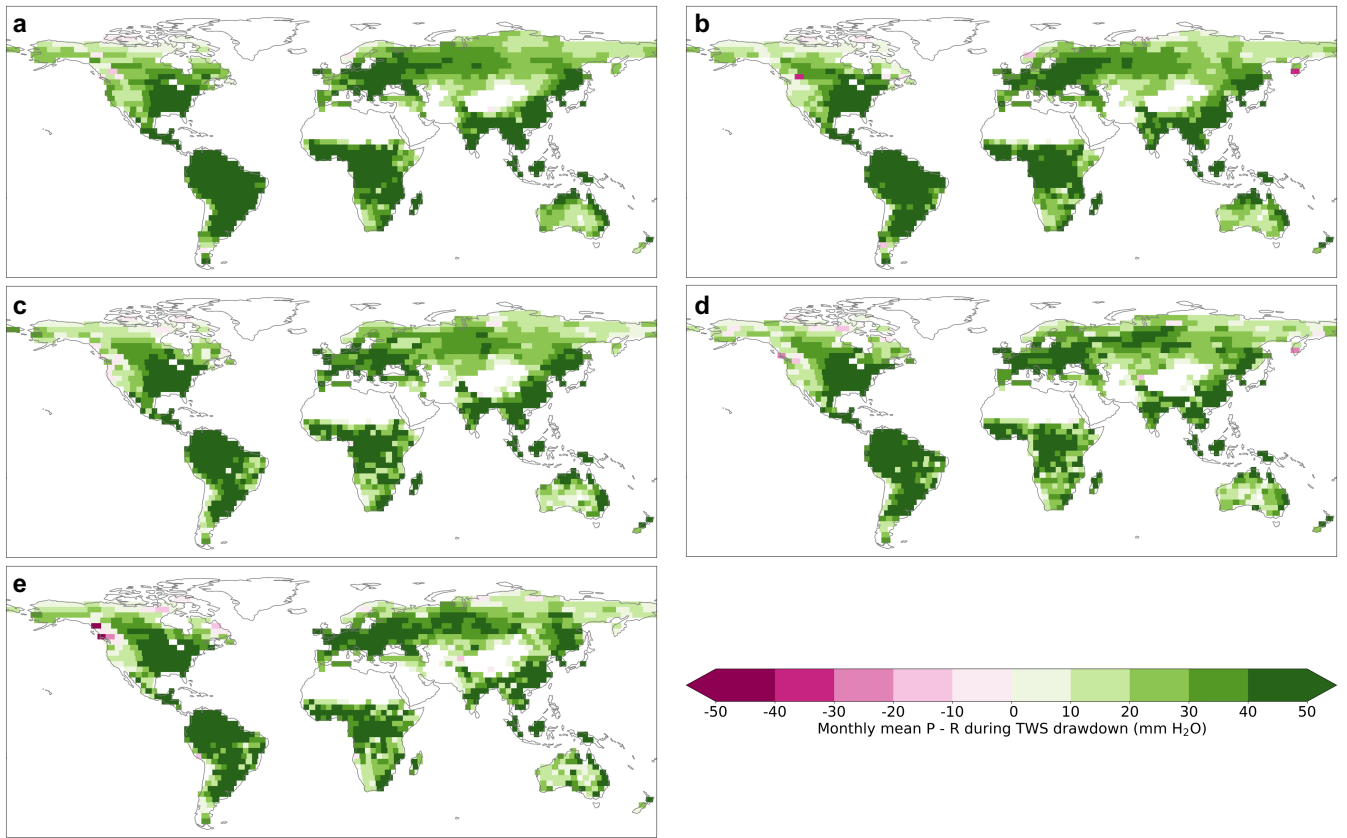
#### 4.5 Implications for high-resolution land surface models

Despite the coarse resolution of GRACE/FO observations,  $S_r^{GRACE/FO}$  and our proposed approach remain valuable for improving the operational configuration of higher-resolution land models. First,  $S_r^{GRACE/FO}$  can be used to evaluate and refine default  $S_r$  parameterizations within models once aggregated to coarse scale of GRACE/FO data, in conjunction with other diagnostic analyses. For instance, if a model underestimates ET during droughts in a region where its  $S_r$  value is significantly lower than  $S_r^{GRACE/FO}$ , the default  $S_r$  value may be increased based on  $S_r^{GRACE/FO}$  even if the model's resolution is much higher than that of  $S_r^{GRACE/FO}$ . Second, in the future, our methodology can be applied extended to downscaled TWSGRACE/FO products, leveraging techniques such as data assimilation systems or artificial intelligence (Li et al., 2019; Gou and Soja, 2024), to improve the characterization of  $S_r$  and its impact on the water and carbon cycles at a higher spatial resolution. of  $S_r^{GRACE/FO}$  (Li et al., 2019; Gou and Soja, 2024).

#### 5 Conclusions

We used GRACE/FO TWS observations to ~~provide a direct observational constraint on~~ estimate root-zone water storage capacity ( $S_r$ ), an essential yet challenging-to-observe variable. The overall ~~better~~ improved performance of  $HydroModel(S_r^{GRACE/FO})$  in simulating ~~TWS and ET observations and the superior  $S_r^{GRACE/FO}$  relationship with  $GPP_{max}$  altogether imply~~ ET, particularly during droughts, implies that  $S_r^{GRACE/FO}$  more accurately reflects the real-world root-zone water storage capacity compared to  $S_r^{RD \times WHC}$  and  $S_r^{accum}$ . ~~These~~ Overall, our results suggest that  $S_r$  is, on average, at least 50% larger than the water deficit-based estimate and by a staggering 380% compared to the rooting depth-based estimate. The underestimations by  $S_r^{accum}$  and  $S_r^{RD \times WHC}$  exceed the random error of  $S_r^{GRACE/FO}$ , underscoring the need for continued refinement and validation of  $S_r$ . Underestimating  $S_r$  may lead to overestimating ecosystem sensitivity to water stress, potentially biasing predictions of future carbon cycle (Ukkola et al., 2021; Giardina et al., 2023). Given the strong coupling between the carbon and water cycles, underestimating  $S_r$  may also lead to underestimating ecosystem water consumption and overestimating human-available water resources, particularly during droughts and heat waves, with important implications for water resource planning (Zhao et al., 2022; Mastrotheodoros et al., 2020).

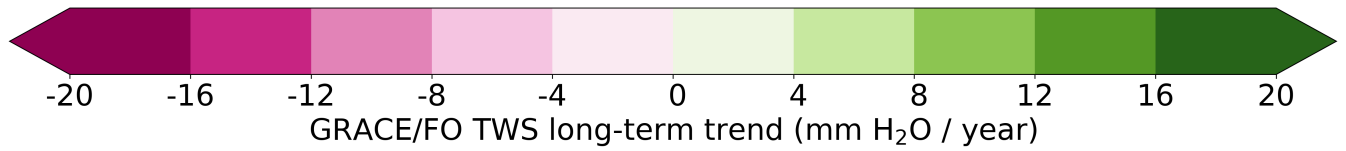
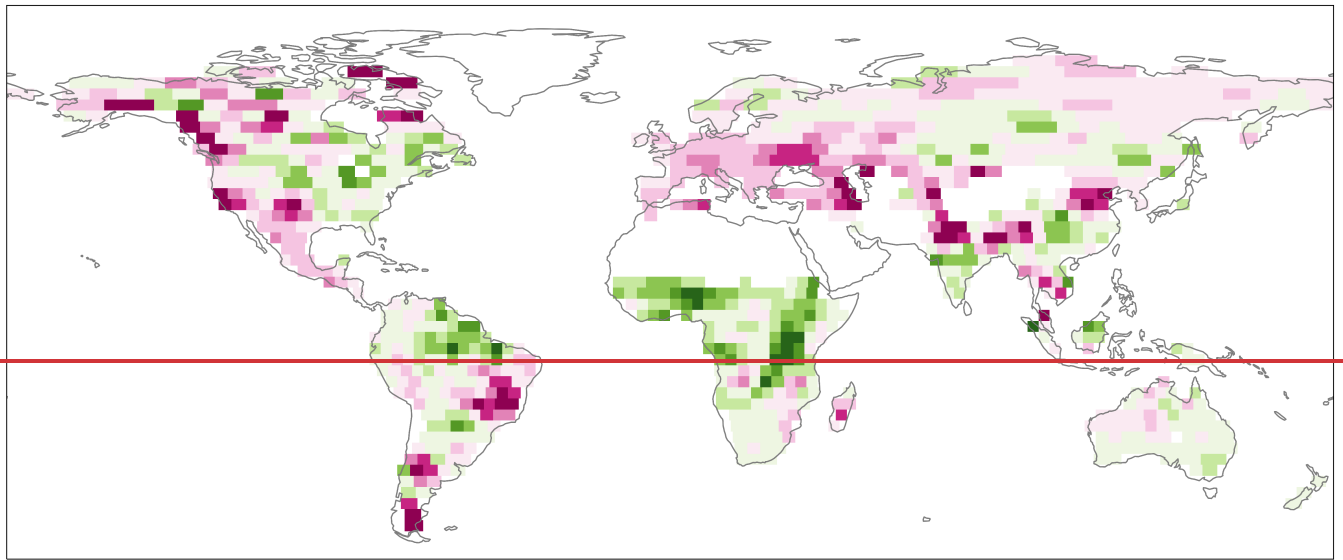




508

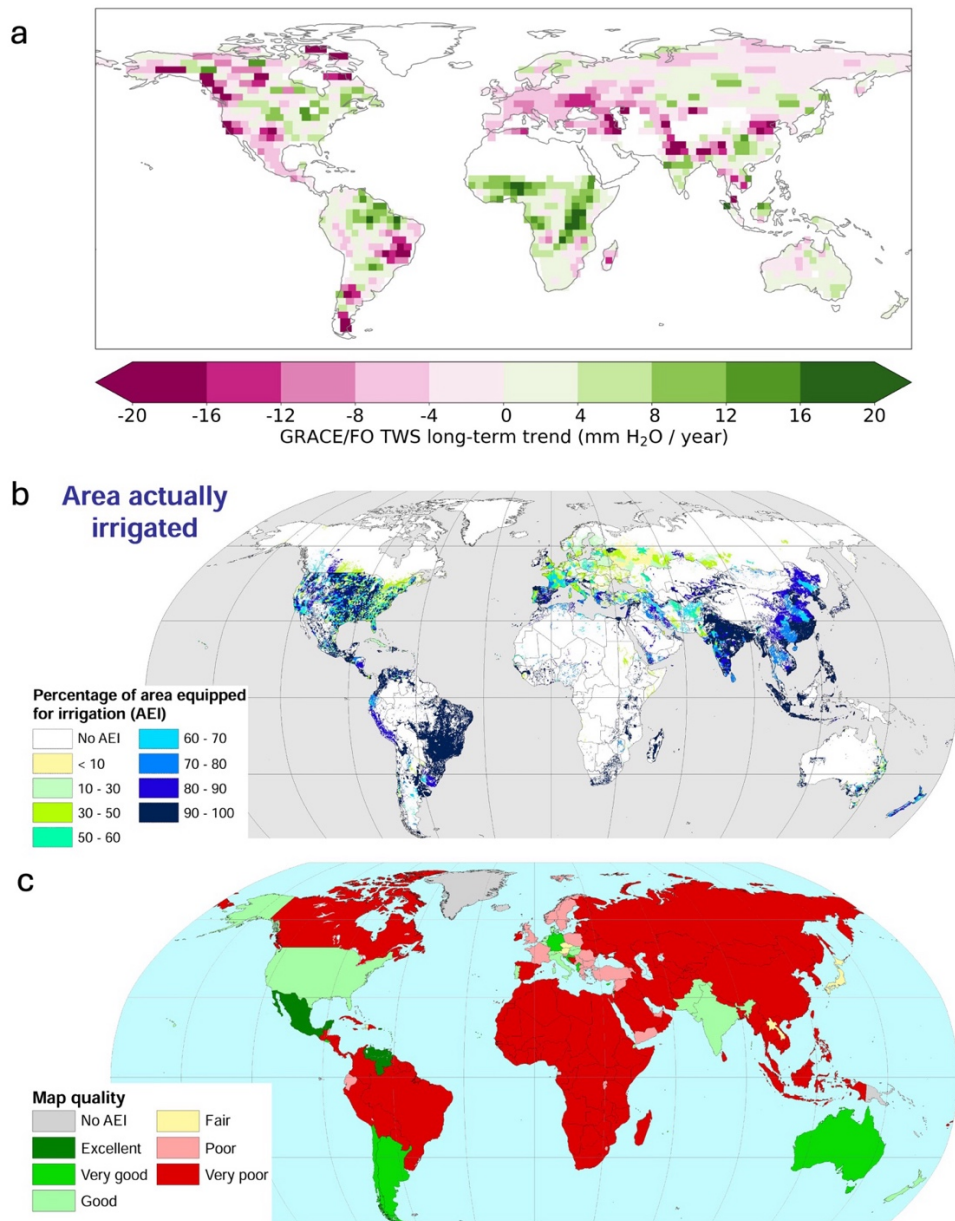
509 **Figure A1.** The ~~cumulative sum of average~~ P - R during the largest (a), the second largest (b), the third largest (c), the fourth  
 510 largest (d), and the fifth largest (e) TWS drawdowns.

511



512





513

514 **Figure A2.** (a) Trends in TWS obtained from GRACE/FO observations from 2002 to 2022.

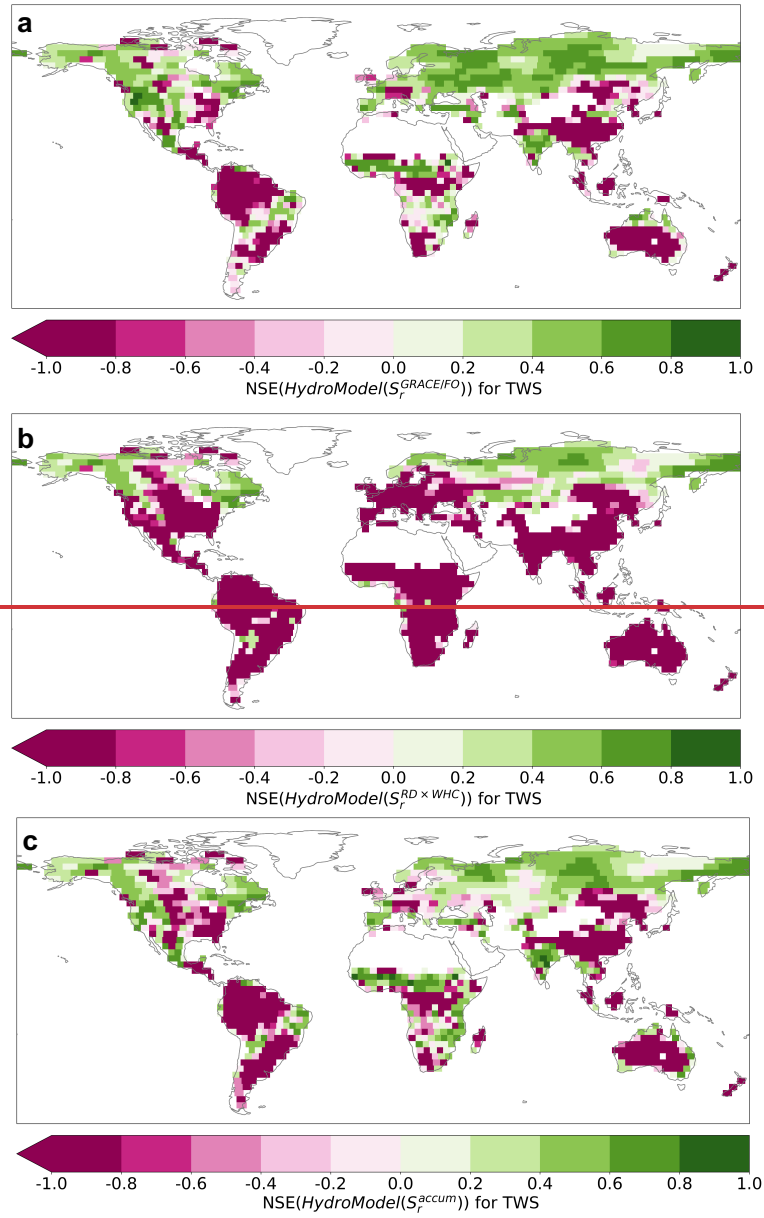


**Figure A3.** NSE values (a) Percentage of area equipped for simulating GRACE/FO TWS by  $\text{HydroModel}(S_r^{\text{GRACE/FO}})$  (a),  $\text{HydroModel}(S_r^{\text{RD} \times \text{WHC}})$  (b), and  $\text{HydroModel}(S_r^{\text{accum}})$  (c), respectively.

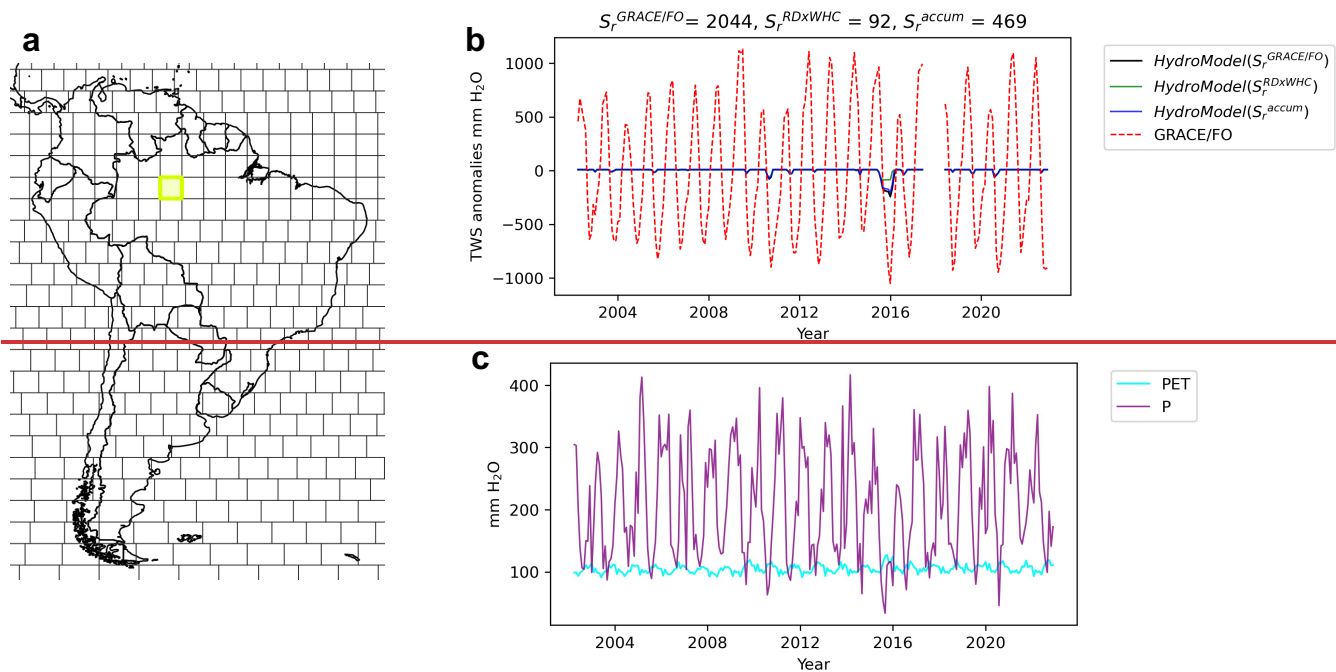


**Figure A4. Model results)** Map quality marks assigned to each country for a very wet maseon area equipped for irrigation in (b). (b-c) are from the Amazon rainforest (a). (b) The comparison between modeled TWS and GRACE/FO TWS. (c) The comparison between the precipitation (P) forcing and model-simulated potential evapotranspiration (PET)-Global Map of Irrigation Areas – version 5.0 by AQUASTA.

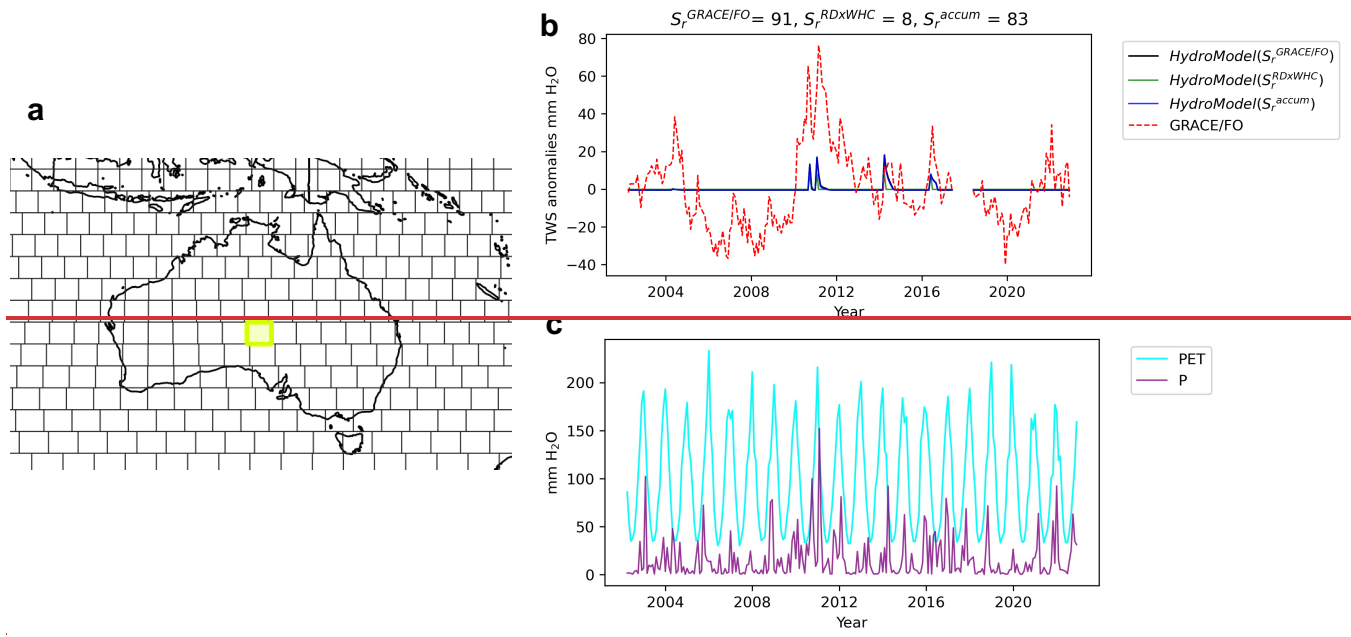


**Figure A5.** Same as Fig. A4 but for a very dry mascon in Australia.

527 **Code availability**

528 The working code to retrieve  $S_r$  from GRACE/FO is available to reviewers. The final code will be archived on Zenodo upon  
529 acceptance of the paper. A DOI link to the archived code will be provided in the final version of the manuscript.

530 **Data availability**

531 The  $S_r^{GRACE/FO}$  will be archived on Zenodo and a DOI link will be provided in the final version of the manuscript. GRACE and  
532 GRACE-FO TWS data are available from the NASA JPL ([https://grace.jpl.nasa.gov/data/get-data/jpl\\_global\\_mascons/](https://grace.jpl.nasa.gov/data/get-data/jpl_global_mascons/)). The  
533 GPCP version 2.3 combined precipitation dataset is available at <https://psl.noaa.gov/data/gridded/data.gpcp.html>. ERA5  
534 reanalysis is available at <https://www.ecmwf.int/en/forecasts/datasets/reanalysis-datasets/era5>. MODIS land cover data are  
535 available at <https://lpdaac.usgs.gov/products/mcd12c1v006/>. Water-balance-based ET data is available at  
536 <https://doi.org/10.5281/zenodo.8339655>. G-RUN global runoff reconstruction data is available at  
537 [https://figshare.com/articles/dataset/GRUN\\_Global\\_Runoff\\_Reconstruction/9228176](https://figshare.com/articles/dataset/GRUN_Global_Runoff_Reconstruction/9228176). **GLEAM ET version 4.1 is available at**  
538 <https://www.gleam.eu/>.

539 **Author contribution**

540 MZ: Conceptualization; Data curation; Formal analysis; Funding acquisition; Methodology; Writing - original draft. ELM:  
541 Methodology; Writing - review & editing. GA: Methodology; Writing - review & editing. AGK: Writing - review & editing.  
542 BL: Writing - review & editing.

543 **Competing interest**

544 The authors declare that they have no conflict of interest.

545 **Acknowledgments**

546 This study was funded by the USGS grant G24AP00031 to the University of Idaho. In addition, ELM was funded by the NSF  
547 Graduate Research Fellowship program and AGK was funded by the NSF DEB 1942133 and the Alfred P. Solan Foundation.

548 **References**

549 Bachofen, C., Tumber-Dávila, S. J., Mackay, D. S., McDowell, N. G., Carminati, A., Klein, T., Stocker, B. D., Mencuccini,  
550 M., and Grossiord, C.: Tree water uptake patterns across the globe, New Phytologist, 242, 1891-1910,  
551 <https://doi.org/10.1111/nph.19762>, 2024.

552 Baldocchi, D., Ma, S., and Verfaillie, J.: On the inter- and intra-annual variability of ecosystem evapotranspiration and water  
553 use efficiency of an oak savanna and annual grassland subjected to booms and busts in rainfall, Global Change Biology, 27,  
554 359-375, <https://doi.org/10.1111/gcb.15414>, 2021.

555 Balland, V., Pollacco, J. A., and Arp, P. A.: Modeling soil hydraulic properties for a wide range of soil conditions, Ecological  
556 Modelling, 219, 300-316, 2008.

557 ~~Biederman, J. A., Scott, R. L., Goulden, M. L., Vargas, R., Litvak, M. E., Kolb, T. E., Yopez, E. A., Oechel, W. C., Blanken,~~  
558 ~~P. D., Bell, T. W., Garatuza Payan, J., Maurer, G. E., Dore, S., and Burns, S. P.: Terrestrial carbon balance in a drier world:~~  
559 ~~the effects of water availability in southwestern North America, Global Change Biology, 22, 1867-1879,~~  
560 ~~<https://doi.org/10.1111/gcb.13222>, 2016.~~

561 Callahan, R. P., Riebe, C. S., Sklar, L. S., Pasquet, S., Ferrier, K. L., Hahm, W. J., Taylor, N. J., Grana, D., Flinchum, B. A.,  
562 and Hayes, J. L.: Forest vulnerability to drought controlled by bedrock composition, Nature Geoscience, 15, 714-719, 2022.

563 ~~Chen, T., de Jeu, R. A. M., Liu, Y. Y., van der Werf, G. R., and Dolman, A. J.: Using satellite-based soil moisture to quantify~~  
564 ~~the water-driven variability in NDVI: A case study over mainland Australia, Remote Sensing of Environment, 140, 330-338,~~  
565 ~~<https://doi.org/10.1016/j.rse.2013.08.022>, 2014.~~

566 ~~Chen, Y., Velicogna, I., Famiglietti, J. S., and Randerson, J. T.: Satellite observations of terrestrial water storage provide early~~  
567 ~~warning information about drought and fire season severity in the Amazon, Journal of Geophysical Research: Biogeosciences,~~  
568 ~~118, 495-504, <https://doi.org/10.1002/jgrg.20046>, 2013.~~

569 ~~Coeley, S. S., FisherDong, J.-B., Lei, F., and Goldsmith, G. R.: ConvergenceCrow, W. T.: Land transpiration-evaporation~~  
570 ~~partitioning errors responsible for modeled summertime warm bias in water use efficiency within plant functional types across~~  
571 ~~contrasting climates the central United States, Nature Plants, 8, 341-345Communications, 13, 336, 10.1038/s41477-022-01131-~~  
572 ~~zs41467-021-27938-6, 2022.~~

573 Espeleta, J. F., West, J. B., and Donovan, L. A.: Species-specific patterns of hydraulic lift in co-occurring adult trees and  
574 grasses in a sandhill community, Oecologia, 138, 341-349, 10.1007/s00442-003-1460-8, 2004.

575 Esteban, E. J. L., Castilho, C. V., Melgaço, K. L., and Costa, F. R. C.: The other side of droughts: wet extremes and topography  
576 as buffers of negative drought effects in an Amazonian forest, New Phytologist, 229, 1995-2006,  
577 <https://doi.org/10.1111/nph.17005>, 2021.

578 Fan, Y., Miguez-Macho, G., Jobbágy, E. G., Jackson, R. B., and Otero-Casal, C.: Hydrologic regulation of plant rooting depth,  
579 Proceedings of the National Academy of Sciences, 114, 10572-10577, 10.1073/pnas.1712381114, 2017.

580 Federer, C., Vörösmarty, C., and Fekete, B.: Sensitivity of annual evaporation to soil and root properties in two models of  
581 contrasting complexity, Journal of Hydrometeorology, 4, 1276-1290, 2003.

582 Feng, W., Zhong, M., Lemoine, J.-M., Biancale, R., Hsu, H.-T., and Xia, J.: Evaluation of groundwater depletion in North  
583 China using the Gravity Recovery and Climate Experiment (GRACE) data and ground-based measurements, Water Resources  
584 Research, 49, 2110-2118, <https://doi.org/10.1002/wrcr.20192>, 2013.

585 Gao, H., Hrachowitz, M., Schymanski, S. J., Fenicia, F., Sriwongsitanon, N., and Savenije, H. H. G.: Climate controls how  
586 ecosystems size the root zone storage capacity at catchment scale, Geophysical Research Letters, 41, 7916-7923,  
587 <https://doi.org/10.1002/2014GL061668>, 2014.

588 Gao, H., Hrachowitz, M., Wang-Erlandsson, L., Fenicia, F., Xi, Q., Xia, J., Shao, W., Sun, G., and Savenije, H. H. G.: Root  
589 zone in the Earth system, Hydrol. Earth Syst. Sci., 28, 4477-4499, 10.5194/hess-28-4477-2024, 2024.

590 Gebremichael, M., Krajewski, W. F., Morrissey, M., Langerud, D., Huffman, G. J., and Adler, R.: Error Uncertainty Analysis  
591 of GPCP Monthly Rainfall Products: A Data-Based Simulation Study, Journal of Applied Meteorology, 42, 1837-1848,  
592 10.1175/1520-0450(2003)042<1837:Euaogm>2.0.Co;2, 2003.

593 Ghiggi, G., Humphrey, V., Seneviratne, S. I., and Gudmundsson, L.: G-RUN ENSEMBLE: A Multi-Forcing Observation-  
594 Based Global Runoff Reanalysis, Water Resources Research, 57, e2020WR028787, <https://doi.org/10.1029/2020WR028787>,  
595 2021.

596 Giardina, F., Gentine, P., Konings, A. G., Seneviratne, S. I., and Stocker, B. D.: Diagnosing evapotranspiration responses to  
597 water deficit across biomes using deep learning, New Phytologist, n/a, <https://doi.org/10.1111/nph.19197>, 2023.

598 Gou, J. and Soja, B.: Global high-resolution total water storage anomalies from self-supervised data assimilation using deep  
599 learning algorithms, Nature Water, 2, 139-150, 10.1038/s44221-024-00194-w, 2024.

600 Goulden, M. L. and Bales, R. C.: California forest die-off linked to multi-year deep soil drying in 2012–2015 drought, Nature  
601 Geoscience, 12, 632-637, 10.1038/s41561-019-0388-5, 2019.

602 Hahm, W. J., Rempe, D., Dralle, D., Dawson, T., and Dietrich, W.: Oak transpiration drawn from the weathered bedrock  
603 vadose zone in the summer dry season, Water Resources Research, 56, e2020WR027419, 2020.

604 Hahm, W. J., Dralle, D. N., Rempe, D. M., Bryk, A. B., Thompson, S. E., Dawson, T. E., and Dietrich, W. E.: Low Subsurface  
605 Water Storage Capacity Relative to Annual Rainfall Decouples Mediterranean Plant Productivity and Water Use From Rainfall  
606 Variability, Geophysical Research Letters, 46, 6544-6553, <https://doi.org/10.1029/2019GL083294>, 2019.

607 Hamon, W. R.: Computation of direct runoff amounts from storm rainfall, 1964.

608 Hain, C. R., Crow, W. T., Anderson, M. C., and Yilmaz, M. T.: Diagnosing Neglected Soil Moisture Source–Sink Processes  
609 via a Thermal Infrared–Based Two-Source Energy Balance Model, Journal of Hydrometeorology, 16, 1070-1086,  
610 <https://doi.org/10.1175/JHM-D-14-0017.1>, 2015.

611 Hersbach, H., Bell, B., Berrisford, P., Hirahara, S., Horányi, A., Muñoz-Sabater, J., Nicolas, J., Peubey, C., Radu, R., Schepers,  
612 D., Simmons, A., Soci, C., Abdalla, S., Abellan, X., Balsamo, G., Bechtold, P., Biavati, G., Bidlot, J., Bonavita, M., De Chiara,  
613 G., Dahlgren, P., Dee, D., Diamantakis, M., Dragani, R., Flemming, J., Forbes, R., Fuentes, M., Geer, A., Haimberger, L.,  
614 Healy, S., Hogan, R. J., Hólm, E., Janisková, M., Keeley, S., Laloyaux, P., Lopez, P., Lupu, C., Radnoti, G., de Rosnay, P.,  
615 Rozum, I., Vamborg, F., Villaume, S., and Thépaut, J.-N.: The ERA5 global reanalysis, Quarterly Journal of the Royal  
616 Meteorological Society, 146, 1999-2049, <https://doi.org/10.1002/qj.3803>, 2020.

617 Hsu, J. S., Powell, J., and Adler, P. B.: Sensitivity of mean annual primary production to precipitation, Global Change Biology,  
618 48, 2246–2255, <https://doi.org/10.1111/j.1365-2486.2012.02687.x>, 2012.

619 Hulsman, P., Keune, J., Koppa, A., Schellekens, J., and Miralles, D. G.: Incorporating Plant Access to Groundwater in Existing  
620 Global, Satellite-Based Evaporation Estimates, Water Resources Research, 59, e2022WR033731,  
621 <https://doi.org/10.1029/2022WR033731>, 2023.

622 Humphrey, V., Zscheischler, J., Ciais, P., Gudmundsson, L., Sitch, S., and Seneviratne, S. I.: Sensitivity of atmospheric CO<sub>2</sub>  
623 growth rate to observed changes in terrestrial water storage, Nature, 560, 628-631, 10.1038/s41586-018-0424-4, 2018.



624 ~~Huxman, T. E., Smith, M. D., Fay, P. A., Knapp, A. K., Shaw, M. R., Loik, M. E., Smith, S. D., Tissue, D. T., Zak, J. C.,~~  
625 ~~Weltzin, J. F., Pockman, W. T., Sala, O. E., Haddad, B. M., Harte, J., Koch, G. W., Schwinning, S., Small, E. E., and Williams,~~  
626 ~~D. G.: Convergence across biomes to a common rain use efficiency, *Nature*, 429, 651–654, [10.1038/nature02561](https://doi.org/10.1038/nature02561), 2004.~~

627 Jackson, R. B., Moore, L. A., Hoffmann, W. A., Pockman, W. T., and Linder, C. R.: Ecosystem rooting depth determined with  
628 caves and DNA, *Proceedings of the National Academy of Sciences*, 96, 11387–11392, doi:10.1073/pnas.96.20.11387, 1999.

629 ~~Jensen, L., Eicker, A., Dobslaw, H., Stacke, T., and Humphrey, V.: Long Term Wetting and Drying Trends in Land Water~~  
630 ~~Storage Derived From GRACE and CMIP5 Models, *Journal of Geophysical Research: Atmospheres*, 124, 9808–9823,~~  
631 ~~<https://doi.org/10.1029/2018JD029989>, 2019.~~

632 ~~Joiner, J. and Yoshida, Y.: Satellite-based reflectances capture large fraction of variability in global gross primary production~~  
633 ~~(GPP) at weekly time scales, *Agricultural and Forest Meteorology*, 291, 108092, 2020.~~

634 ~~Joiner, J. and Yoshida, Y.: Global MODIS and FLUXNET derived Daily Gross Primary Production, V2,~~  
635 ~~[10.3334/ORNLDAAC/1835](https://doi.org/10.3334/ORNLDAAC/1835), 2021.~~

636 ~~Jiménez-Rodríguez, C. D., Sulis, M., and Schymanski, S.: Exploring the role of bedrock representation on plant transpiration~~  
637 ~~response during dry periods at four forested sites in Europe, *Biogeosciences*, 19, 3395–3423, 2022.~~

638 ~~Koirala, S., Jung, M., Reichstein, M., de Graaf, I. E. M., Camps-Valls, G., Ichii, K., Papale, D., Ráduly, B., Schwalm, C. R.,~~  
639 ~~Tramontana, G., and Carvalhais, N.: Global distribution of groundwater-vegetation spatial covariation, *Geophysical Research*~~  
640 ~~Letters, 44, 4134–4142, <https://doi.org/10.1002/2017GL072885>, 2017.~~

641 ~~Koppa, A., Rains, D., Hulsman, P., Poyatos, R., and Miralles, D. G.: A deep learning-based hybrid model of global terrestrial~~  
642 ~~evaporation, *Nature Communications*, 13, 1912, [10.1038/s41467-022-29543-7](https://doi.org/10.1038/s41467-022-29543-7), 2022.~~

643 ~~Kuzyakov, Y. and Razavi, B. S.: Rhizosphere size and shape: Temporal dynamics and spatial stationarity, *Soil Biology and*~~  
644 ~~*Biochemistry*, 135, 343–360, <https://doi.org/10.1016/j.soilbio.2019.05.011>, 2019.~~

645 ~~Li, B., Rodell, M., and Famiglietti, J. S.: Groundwater variability across temporal and spatial scales in the central and~~  
646 ~~northeastern U.S, *Journal of Hydrology*, 525, 769–780, <https://doi.org/10.1016/j.jhydrol.2015.04.033>, 2015.~~

647 Li, B., Rodell, M., Kumar, S., Beaudoin, H. K., Getirana, A., Zaitchik, B. F., de Goncalves, L. G., Cossetin, C., Bhanja, S.,  
648 and Mukherjee, A.: Global GRACE data assimilation for groundwater and drought monitoring: Advances and challenges,  
649 *Water Resources Research*, 55, 7564–7586, 2019.

650 Liu, P.-W., Famiglietti, J. S., Purdy, A. J., Adams, K. H., McEvoy, A. L., Reager, J. T., Bindlish, R., Wiese, D. N., David, C.  
651 H., and Rodell, M.: Groundwater depletion in California’s Central Valley accelerates during megadrought, *Nature*  
652 *Communications*, 13, 7825, [10.1038/s41467-022-35582-x](https://doi.org/10.1038/s41467-022-35582-x), 2022.

653 Livneh, B. and Hoerling, M. P.: The Physics of Drought in the U.S. Central Great Plains, *Journal of Climate*, 29, 6783–6804,  
654 <https://doi.org/10.1175/JCLI-D-15-0697.1>, 2016.

655 Mastrotheodoros, T., Pappas, C., Molnar, P., Burlando, P., Manoli, G., Parajka, J., Rigon, R., Szeles, B., Bottazzi, M.,  
656 Hadjidoukas, P., and Fatichi, S.: More green and less blue water in the Alps during warmer summers, *Nature Climate Change*,  
657 10, 155–161, [10.1038/s41558-019-0676-5](https://doi.org/10.1038/s41558-019-0676-5), 2020.

658 Maxwell, R. M. and Condon, L. E.: Connections between groundwater flow and transpiration partitioning, *Science*, 353, 377–  
659 380, doi:10.1126/science.aaf7891, 2016.

660 McCabe, G. J. and Markstrom, S. L.: A monthly water-balance model driven by a graphical user interface, US Geological  
661 Survey Reston, VA, USA2007.

662 ~~McCabe, G. J., Hay, L. E., Boek, A., Markstrom, S. L., and Atkinson, R. D.: Inter annual and spatial variability of Hamon~~  
663 ~~potential — evapotranspiration — model — coefficients, — Journal — of — Hydrology, — 521, — 389-394,~~  
664 ~~<https://doi.org/10.1016/j.jhydrol.2014.12.006>, 2015.~~

665 McCormick, E. L., Dralle, D. N., Hahm, W. J., Tune, A. K., Schmidt, L. M., Chadwick, K. D., and Rempe, D. M.: Widespread  
666 woody plant use of water stored in bedrock, *Nature*, 597, 225-229, 10.1038/s41586-021-03761-3, 2021.

667 ~~McKee, T. B., Doesken, N. J., and Kleist, J.: The relationship of drought frequency and duration to time scales, *Proceedings*~~  
668 ~~*of the 8th Conference on Applied Climatology*, 179-183,~~

669 Miguez-Macho, G. and Fan, Y.: Spatiotemporal origin of soil water taken up by vegetation, *Nature*, 598, 624-628,  
670 10.1038/s41586-021-03958-6, 2021.

671 Miralles, D. G., ~~Bonte, O., Koppa, A., Villanueva, O. B., Tronquo, E., Zhong, F., Beck, H., Hulsman, P., Dorigo, W., and~~  
672 ~~Verhoest, N. E.: GLEAM4: global land evaporation dataset at 0.1 resolution from 1980 to near present, 2024.~~

673 ~~Miralles, D. G.,~~ Jiménez, C., Jung, M., Michel, D., Ershadi, A., McCabe, M. F., Hirschi, M., Martens, B., Dolman, A. J.,  
674 Fisher, J. B., Mu, Q., Seneviratne, S. I., Wood, E. F., and Fernández-Prieto, D.: The WACMOS-ET project – Part 2: Evaluation  
675 of global terrestrial evaporation data sets, *Hydrol. Earth Syst. Sci.*, 20, 823-842, 10.5194/hess-20-823-2016, 2016.

676 Nash, J. E. and Sutcliffe, J. V.: River flow forecasting through conceptual models part I—A discussion of principles, *Journal*  
677 *of hydrology*, 10, 282-290, 1970.

678 ~~Naumburg, E., Mata-gonzalez, R., Hunter, R. G., McLendon, T., and Martin, D. W.: Phreatophytic Vegetation and~~  
679 ~~Groundwater Fluctuations: A Review of Current Research and Application of Ecosystem Response Modeling with an~~  
680 ~~Emphasis on Great Basin Vegetation, *Environmental Management*, 35, 726-740, 10.1007/s00267-004-0194-7, 2005.~~

681 Novick, K. A., Ficklin, D. L., Baldocchi, D., Davis, K. J., Ghezzehei, T. A., Konings, A. G., MacBean, N., Raoult, N., Scott,  
682 R. L., Shi, Y., Sulman, B. N., and Wood, J. D.: Confronting the water potential information gap, *Nature Geoscience*, 15, 158-  
683 164, 10.1038/s41561-022-00909-2, 2022.

684 ~~Paseolini-Campbell, M. A., Reager, J. T., and Fisher, J. B.: GRACE-based Mass Conservation as a Validation Target for~~  
685 ~~Basin-Scale Evapotranspiration in the Contiguous United States, *Water Resources Research*, 56, e2019WR026594,~~  
686 ~~<https://doi.org/10.1029/2019WR026594>, 2020.~~

687 ~~Orellana, F., Verma, P., Loheide II, S. P., and Daly, E.: Monitoring and modeling water-vegetation interactions in groundwater-~~  
688 ~~dependent ecosystems, *Reviews of Geophysics*, 50, <https://doi.org/10.1029/2011RG000383>, 2012.~~

689 Pérez-Ruiz, E. R., Vivoni, E. R., and Sala, O. E.: Seasonal carryover of water and effects on carbon dynamics in a dryland  
690 ecosystem, *Ecosphere*, 13, e4189, 2022.

691 Peterson, T. J., Saft, M., Peel, M. C., and John, A.: Watersheds may not recover from drought, *Science*, 372, 745-749,  
692 doi:10.1126/science.abd5085, 2021.

693 ~~Ponce-Campos, G. E., Moran, M. S., Huete, A., Zhang, Y., Bresloff, C., Huxman, T. E., Eamus, D., Bosch, D. D., Buda, A.~~  
694 ~~R., Gunter, S. A., Sealley, T. H., Kitchen, S. G., McClaran, M. P., McNab, W. H., Montoya, D. S., Morgan, J. A., Peters, D.~~

695 P. C., Sadler, E. J., Seyfried, M. S., and Starks, P. J.: Ecosystem resilience despite large-scale altered hydroclimatic conditions,  
696 *Nature*, 494, 349–352, 10.1038/nature11836, 2013.

697 Rempe, D. M. and Dietrich, W. E.: Direct observations of rock moisture, a hidden component of the hydrologic cycle,  
698 *Proceedings of the National Academy of Sciences*, 115, 2664–2669, doi:10.1073/pnas.1800141115, 2018.

699 Rodell, M., Velicogna, I., and Famiglietti, J. S.: Satellite-based estimates of groundwater depletion in India, *Nature*, 460, 999–  
700 1002, 10.1038/nature08238, 2009.

701 Rodell, M., Chao, B. F., Au, A. Y., Kimball, J. S., and McDonald, K. C.: Global biomass variation and its geodynamic effects:  
702 1982–98, *Earth Interactions*, 9, 1–19, 2005.

703 Rodell, M., Famiglietti, J. S., ~~Chen, J., Seneviratne, S. I., Viterbo, P., Holl, S., and Wilson, C. R.: Basin-scale estimates of~~  
704 ~~evapotranspiration using GRACE and other observations, *Geophysical Research Letters*, 31,~~  
705 ~~<https://doi.org/10.1029/2004GL020873>, 2004.~~

706 ~~Rodell, M., Famiglietti, J. S.,~~ Wiese, D. N., Reager, J. T., Beaudoin, H. K., Landerer, F. W., and Lo, M. H.: Emerging trends  
707 in global freshwater availability, *Nature*, 557, 651–659, 10.1038/s41586-018-0123-1, 2018.

708 ~~Scanlon, B. R., Zhang, Z., Save, H., Sun, A. Y., Müller-Schmied, H., van Beek, L. P. H., Wiese, D. N., Wada, Y., Long, D.,~~  
709 ~~Reedy, R. C., Longuevergne, L., Döll, P., and Bierkens, M. F. P.: Global models underestimate large decadal declining and~~  
710 ~~rising water storage trends relative to GRACE satellite data, *Proceedings of the National Academy of Sciences*, 115, E1080–~~  
711 ~~E1089, doi:10.1073/pnas.1704665115, 2018.~~

712 ~~Rohde, M. M., Albano, C. M., Huggins, X., Klausmeyer, K. R., Morton, C., Sharman, A., Zaveri, E., Saito, L., Freed, Z.,~~  
713 ~~Howard, J. K., Job, N., Richter, H., Toderich, K., Rodella, A.-S., Gleeson, T., Huntington, J., Chandanpurkar, H. A., Purdy,~~  
714 ~~A. J., Famiglietti, J. S., Singer, M. B., Roberts, D. A., Caylor, K., and Stella, J. C.: Groundwater-dependent ecosystem map~~  
715 ~~exposes global dryland protection needs, *Nature*, 632, 101–107, 10.1038/s41586-024-07702-8, 2024.~~

716 ~~Schlemmer, L., Schär, C., Lüthi, D., and Strebel, L.: A Groundwater and Runoff Formulation for Weather and Climate Models,~~  
717 ~~*Journal of Advances in Modeling Earth Systems*, 10, 1809–1832, <https://doi.org/10.1029/2017MS001260>, 2018.~~

718 Scott, R. L. and Biederman, J. A.: Critical Zone Water Balance Over 13 Years in a Semiarid Savanna, *Water Resources*  
719 *Research*, 55, 574–588, <https://doi.org/10.1029/2018WR023477>, 2019.

720 Seneviratne, S. I., Corti, T., Davin, E. L., Hirschi, M., Jaeger, E. B., Lehner, I., Orlowsky, B., and Teuling, A. J.: Investigating  
721 soil moisture–climate interactions in a changing climate: A review, *Earth-Science Reviews*, 99, 125–161,  
722 <https://doi.org/10.1016/j.earscirev.2010.02.004>, 2010.

723 Speich, M. J., Lischke, H., and Zappa, M.: Testing an optimality-based model of rooting zone water storage capacity in  
724 temperate forests, *Hydrology and Earth System Sciences*, 22, 4097–4124, 2018.

725 Stocker, B. D., Tumber-Dávila, S. J., Konings, A. G., Anderson, M. C., Hain, C., and Jackson, R. B.: Global patterns of water  
726 storage in the rooting zones of vegetation, *Nature Geoscience*, 10.1038/s41561-023-01125-2, 2023.

727 ~~Stoy, P. C., El-Madany, T. S., Fisher, J. B., Gentile, P., Gerken, T., Good, S. P., Klosterhalfen, A., Liu, S., Miralles, D. G.,~~  
728 ~~and Perez-Priego, O.: Reviews and syntheses: Turning the challenges of partitioning ecosystem evaporation and transpiration~~  
729 ~~into opportunities, *Biogeosciences*, 16, 3747–3775, 2019.~~

- 730 Sulla-Menashe, D. and Friedl, M. A.: User guide to collection 6 MODIS land cover (MCD12Q1 and MCD12C1) product,  
731 USGS: Reston, VA, USA, 1-18, 2018.
- 732 Sun, G., Zuo, C., Liu, S., Liu, M., McNulty, S. G., and Vose, J. M.: Watershed Evapotranspiration Increased due to Changes  
733 in Vegetation Composition and Structure Under a Subtropical Climate1, JAWRA Journal of the American Water Resources  
734 Association, 44, 1164-1175, <https://doi.org/10.1111/j.1752-1688.2008.00241.x>, 2008.
- 735 Sun, Q., Miao, C., Duan, Q., Ashouri, H., Sorooshian, S., and Hsu, K.-L.: A Review of Global Precipitation Data Sets: Data  
736 Sources, Estimation, and Intercomparisons, Reviews of Geophysics, 56, 79-107, <https://doi.org/10.1002/2017RG000574>,  
737 2018.
- 738 Swann, A. L. S. and Koven, C. D.: A Direct Estimate of the Seasonal Cycle of Evapotranspiration over the Amazon Basin,  
739 Journal of Hydrometeorology, 18, 2173-2185, <https://doi.org/10.1175/JHM-D-17-0004.1>, 2017.
- 740 Swenson, S. and Wahr, J.: Estimating large-scale precipitation minus evapotranspiration from GRACE satellite gravity  
741 measurements, Journal of Hydrometeorology, 7, 252-270, 2006.
- 742 Tang, R., Peng, Z., Liu, M., Li, Z. L., Jiang, Y., Hu, Y., Huang, L., Wang, Y., Wang, J., and Jia, L.: Spatial-temporal patterns  
743 of land surface evapotranspiration from global products, Remote Sensing of Environment, 304, 114066, 2024.
- 744 Teuling, A. J., Seneviratne, S. I., Williams, C., and Troch, P. A.: Observed timescales of evapotranspiration response to soil  
745 moisture, Geophysical Research Letters, 33, <https://doi.org/10.1029/2006GL028178>, 2006.
- 746 Trugman, A. T., Medvigy, D., Mankin, J. S., and Anderegg, W. R. L.: Soil Moisture Stress as a Major Driver of Carbon Cycle  
747 Uncertainty, Geophysical Research Letters, 45, 6495-6503, <https://doi.org/10.1029/2018GL078131>, 2018.
- 748 Thompson, S. E., Harman, C. J., Konings, A. G., Sivapalan, M., Neal, A., and Troch, P. A.: Comparative hydrology across  
749 AmeriFlux sites: The variable roles of climate, vegetation, and groundwater, Water Resources Research, 47,  
750 <https://doi.org/10.1029/2010WR009797>, 2011.
- 751 Ukkola, A. M., De Kauwe, M. G., Roderick, M. L., Burrell, A., Lehmann, P., and Pitman, A. J.: Annual precipitation explains  
752 variability in dryland vegetation greenness globally but not locally, Glob Chang Biol, 27, 4367-4380, 10.1111/gcb.15729,  
753 2021.
- 754 Velicogna, I., Tong, J., Zhang, T., and Kimball, J. S.: Increasing subsurface water storage in discontinuous permafrost areas  
755 of the Lena River basin, Eurasia, detected from GRACE, Geophysical Research Letters, 39,  
756 <https://doi.org/10.1029/2012GL051623>, 2012.
- 757 Vereecken, H., Amelung, W., Bauke, S. L., Bogen, H., Brüggemann, N., Montzka, C., Vanderborght, J., Bechtold, M.,  
758 Blöschl, G., Carminati, A., Javaux, M., Konings, A. G., Kusche, J., Neuweiler, I., Or, D., Steele-Dunne, S., Verhoef, A.,  
759 Young, M., and Zhang, Y.: Soil hydrology in the Earth system, Nature Reviews Earth & Environment, 3, 573-587,  
760 10.1038/s43017-022-00324-6, 2022.
- 761 Wang, S., Li, J., and Russell, H. A. J.: Methods for Estimating Surface Water Storage Changes and Their Evaluations, Journal  
762 of Hydrometeorology, 24, 445-461, <https://doi.org/10.1175/JHM-D-22-0098.1>, 2023a.
- 763 Wang, T., Wu, Z., Wang, P., Wu, T., Zhang, Y., Yin, J., Yu, J., Wang, H., Guan, X., Xu, H., Yan, D., and Yan, D.: Plant-  
764 groundwater interactions in drylands: A review of current research and future perspectives, Agricultural and Forest  
765 Meteorology, 341, 109636, <https://doi.org/10.1016/j.agrformet.2023.109636>, 2023b.

766 Wang-Erlandsson, L., Bastiaanssen, W. G. M., Gao, H., Jägermeyr, J., Senay, G. B., van Dijk, A. I. J. M., Guerschman, J. P.,  
767 Keys, P. W., Gordon, L. J., and Savenije, H. H. G.: Global root zone storage capacity from satellite-based evaporation, Hydrol.  
768 Earth Syst. Sci., 20, 1459-1481, 10.5194/hess-20-1459-2016, 2016.

769 Watkins, M. M., Wiese, D. N., Yuan, D.-N., Boening, C., and Landerer, F. W.: Improved methods for observing Earth's time  
770 variable mass distribution with GRACE using spherical cap mascons, Journal of Geophysical Research: Solid Earth, 120,  
771 2648-2671, <https://doi.org/10.1002/2014JB011547>, 2015.

772 Wieder, W., Boehnert, J., Bonan, G., and Langseth, M.: RegridDED Harmonized World Soil Database v1. 2. Data Set. Available  
773 on-Line [[Http://Daac. Ornl. Gov](http://Daac.Ornl.Gov)] from Oak Ridge National Laboratory Distributed Active Archive Center, Oak Ridge,  
774 Tennessee, USA, 2014.

775 Wiese, D. N., Landerer, F. W., and Watkins, M. M.: Quantifying and reducing leakage errors in the JPL RL05M GRACE  
776 mascon solution, Water Resources Research, 52, 7490-7502, <https://doi.org/10.1002/2016WR019344>, 2016.

777 ~~Xiong, J., Abhishek, Xu, L., Chandanpurkar, H. A., Famiglietti, J. S., Zhang, C., Ghiggi, G., Guo, S., Pan, Y., and~~  
778 ~~Vishwakarma, B. D.: ET-WB: water balance-based estimations of terrestrial evaporation over global land and major global~~  
779 ~~basins, Earth System Science Data Discussions, 2023, 1-47, 2023.~~

780 Yang, Y., Donohue, R. J., and McVicar, T. R.: Global estimation of effective plant rooting depth: Implications for hydrological  
781 modeling, Water Resources Research, 52, 8260-8276, <https://doi.org/10.1002/2016WR019392>, 2016.

782 Zhao, M., A, G., Liu, Y., and Konings, A. G.: Evapotranspiration frequently increases during droughts, Nature Climate  
783 Change, 12, 1024-1030, 10.1038/s41558-022-01505-3, 2022.

784 Zhao, M., A, G., Zhang, J., Velicogna, I., Liang, C., and Li, Z.: Ecological restoration impact on total terrestrial water storage,  
785 Nature Sustainability, 4, 56-62, 10.1038/s41893-020-00600-7, 2021.

786